

1 Comparison of aqueous SOA product distributions from guaiacol 2 oxidation by non-phenolic and phenolic methoxybenzaldehydes as 3 photosensitizers in the absence and presence of ammonium nitrate

4 Beatrix Rosette Go Mabato^{1,2}, Yong Jie Li³, Dan Dan Huang⁴, Yalin Wang³, and Chak K. Chan^{1,2*}

5 ¹School of Energy and Environment, City University of Hong Kong, Hong Kong, China

6 ²City University of Hong Kong Shenzhen Research Institute, Shenzhen, China

7 ³Department of Civil and Environmental Engineering, and Centre for Regional Ocean, Faculty of Science and Technology,
8 University of Macau, Macau, China

9 ⁴Shanghai Academy of Environmental Sciences, Shanghai 200233, China

10

11 *Correspondence to:* Chak K. Chan (Chak.K.Chan@cityu.edu.hk)

12 **Abstract.** Aromatic carbonyls (e.g., methoxybenzaldehydes), an important class of photosensitizers, are abundant in the
13 atmosphere. Photosensitization and nitrate-mediated photo-oxidation can occur simultaneously, yet studies about their
14 interactions, particularly for aqueous secondary organic aerosol (aqSOA) formation, remain limited. This study compared
15 non-phenolic (3,4-dimethoxybenzaldehyde, DMB) and phenolic (vanillin, VL) methoxybenzaldehydes as photosensitizers
16 for aqSOA formation via guaiacol (GUA) oxidation in the absence and presence of ammonium nitrate (AN) under
17 atmospherically relevant cloud and fog conditions. GUA oxidation by triplet excited states of DMB (³DMB*) (GUA+DMB)
18 was ~4 times faster and exhibited greater light absorption than oxidation by ³VL* (GUA+VL). Both GUA+DMB and
19 GUA+VL formed aqSOA composed of oligomers, functionalized monomers, oxygenated ring-opening species, and N-
20 containing products in the presence of AN. The observation of N-heterocycles such as imidazoles indicates the participation
21 of ammonium in the reactions. The majority of generated aqSOA are potential brown carbon (BrC) chromophores.
22 Oligomerization and functionalization dominated in GUA+DMB and GUA+VL, but functionalization appeared to be more
23 important in GUA+VL due to contributions from VL itself. AN did not significantly affect the oxidation kinetics, but it had
24 distinct effects on the product distributions, likely due to differences in the photosensitizing abilities and structural features
25 of DMB and VL. In particular, the more extensive fragmentation in GUA+DMB than in GUA+VL likely generated more N-
26 containing products in GUA+DMB+AN. In GUA+VL+AN, the increased oligomers may be due to VL-derived phenoxy
27 radicals induced by [•]OH or [•]NO₂ from nitrate photolysis. Furthermore, increased nitrated products observed in the presence
28 of both DMB or VL and AN than in AN alone implies that photosensitized reactions may promote nitration. This work
29 demonstrates how the structural features of photosensitizers affect aqSOA formation via non-carbonyl phenol oxidation.
30 Potential interactions between photosensitization and AN photolysis were also elucidated. These findings facilitate a better
31 understanding of photosensitized aqSOA formation and highlight the importance of AN photolysis in these reactions.

32 1 Introduction

33 Photosensitized reactions involving triplet excited states of organic compounds ($^3\text{C}^*$) are efficient pathways for the
34 formation of secondary organic aerosol in the aqueous phase (aqSOA; Smith et al., 2014, 2016; Yu et al., 2014, 2016; Chen
35 et al., 2020; Jiang et al., 2021; Misovich et al., 2021; Mabato et al., 2022). Upon irradiation by solar radiation,
36 photosensitizers form an excited triplet state that directly reacts with substrates (e.g., phenols), and can generate singlet
37 oxygen ($^1\text{O}_2$), superoxide ($\text{O}_2^{\cdot-}$) or hydroperoxyl ($^{\cdot}\text{HO}_2$) radicals, and hydroxyl radicals ($^{\cdot}\text{OH}$) upon reactions with O_2 and
38 substrates (George et al., 2018; Chen et al., 2020), thereby facilitating the oxidation of rather volatile species and
39 contributing to aqSOA formation. An important class of photosensitizers is aromatic carbonyls (e.g.,
40 methoxybenzaldehydes) which are abundant in aerosol particles, cloud waters, and fog waters (Anastasio et al., 1997; Felber
41 et al., 2021). Aromatic carbonyls can be emitted from anthropogenic sources and biomass burning (BB; Lipari et al., 1984;
42 Edye and Richards, 1991; Hawthorne et al., 1992; Simoneit et al., 1993, 1999; Anastasio et al., 1997; Felber et al., 2021), or
43 formed via atmospheric oxidation of aromatic hydrocarbons (Hoshino et al., 1978; Calvert and Madronich, 1987; Anastasio
44 et al., 1997; Felber et al., 2021). BB is also a significant source of phenols through lignin pyrolysis (Simpson et al., 2005).
45 Phenolic carbonyls have a hydroxyl ($-\text{OH}$) group on the aromatic ring, whereas non-phenolic carbonyls do not. BB smoke
46 has been reported to have comparable concentrations of phenolic and non-phenolic carbonyls (Simoneit et al., 1993;
47 Anastasio et al., 1997).

48 Most previous studies on aqSOA formation via photosensitized non-carbonyl phenol oxidation have examined 3,4-
49 dimethoxybenzaldehyde (DMB), a non-phenolic methoxybenzaldehyde, as the photosensitizer (Smith et al., 2014, 2015; Yu
50 et al., 2014, 2016; Chen et al., 2020; Jiang et al., 2021; Misovich et al., 2021). By contrast, phenolic carbonyls have been
51 mainly studied as aqSOA precursors via $^{\cdot}\text{OH}$ -, nitrate-, nitrite-, and $^3\text{DMB}^*$ -mediated oxidation (Li et al., 2014; Huang et al.,
52 2018; Pang et al., 2019; Jiang et al., 2021; Misovich et al., 2021). However, strongly light-absorbing phenolic carbonyls
53 (e.g., molar absorptivity above 300 nm $\geq 7 \times 10^3 \text{ M}^{-1} \text{ cm}^{-1}$) can also serve as photosensitizers to promote aqSOA formation
54 (Smith et al., 2016; Mabato et al., 2022). For instance, the direct photosensitized oxidation of phenolic carbonyls (i.e.,
55 oxidation of phenolic carbonyls by their $^3\text{C}^*$ or $^3\text{C}^*$ -derived oxidants) such as vanillin (VL; another methoxybenzaldehyde)
56 efficiently form low-volatility products, with aqSOA mass yields of up to 140% (Smith et al., 2016). Moreover, the aqSOA
57 mass yields from the oxidation of syringol by $^3\text{DMB}^*$ and $^3\text{VL}^*$ are similar (111% and 114%, respectively; Smith et al.,
58 2014, 2016). In addition, we recently reported that the direct photosensitized oxidation of VL and guaiacol oxidation by
59 $^3\text{VL}^*$ yield similar products (oligomers, functionalized monomers, and oxygenated ring-opening products) as observed with
60 $^3\text{DMB}^*$ (Yu et al., 2014; Mabato et al., 2022). Guaiacol is a non-carbonyl BB methoxyphenol with an emission rate from
61 fireplace wood combustion in the range of 172 to 279 mg/kg (Schauer et al., 2001; Simoneit, 2002). The atmospheric
62 reactivity of methoxyphenols has recently been reviewed (Liu et al., 2022). However, our previous experiments (Mabato et
63 al., 2022) were performed at a concentration (0.1 mM VL) higher than what was typically used for DMB (0.005 to 0.01 mM;
64 Smith et al., 2014, 2015; Yu et al., 2014, 2016). Therefore, direct comparisons between photosensitization by $^3\text{DMB}^*$ and

65 $^3\text{VL}^*$ cannot be made. Despite the above findings, much is still unknown about how aqSOA formation proceeds in systems
66 using phenolic carbonyls as photosensitizers.

67 BB aerosols are typically internally mixed with other aerosol components, such as ammonium nitrate (AN;
68 Zielinski et al., 2020). Hence, aromatic carbonyls and phenols may coexist with AN in BB aerosols. Nitrate and ammonium
69 facilitate the formation of aqSOA and brown carbon (BrC) via a number of pathways. Nitrate photolysis can produce $\cdot\text{OH}$
70 and nitrating agents (e.g., $\cdot\text{NO}_2$; Minero et al., 2007; Huang et al., 2018; Mabato et al., 2022; Wang et al., 2022; Yang et al.,
71 2022), and ammonium reacts with carbonyls to yield N-containing heterocycles (e.g., imidazoles) and oligomers capable of
72 UV-Vis light absorption (De Haan et al., 2009, 2011; Nozière et al., 2009, 2010, 2018; Shapiro et al., 2009; Yu et al., 2011;
73 Lee et al., 2013; Powelson et al., 2014; Gen et al., 2018; Grace et al., 2019; Mabato et al., 2019). Furthermore, nitrate
74 photolysis may be an important process for SO_2 oxidation and SOA formation in the particle phase (Gen et al., 2019a,
75 2019b, 2022; Zhang et al., 2020, 2021, 2022), and it can potentially modify the morphology of atmospheric viscous particles
76 (Liang et al., 2021). Yet, understanding of the effects of inorganic nitrate on aqSOA formation remains limited. In addition,
77 aqSOA formation studies involving aromatic carbonyls and phenols have probed either photosensitization or nitrate-
78 mediated photo-oxidation, but these reactions can occur simultaneously. For instance, we previously reported nitrated
79 compounds, including a potential imidazole derivative from the direct photosensitized oxidation of VL in the presence of AN
80 (Mabato et al., 2022). Accordingly, investigations on reaction systems including both photosensitizers and AN may provide
81 further insights into the aqueous-phase processing of BB aerosols.

82 In this work, we compared aqSOA formation from photosensitized guaiacol (GUA) oxidation by $^3\text{C}^*$ of non-
83 phenolic and phenolic methoxybenzaldehydes under identical conditions (simulated sunlight and concentration) relevant to
84 cloud and fog waters. The effects of AN on photosensitized aqSOA formation were also examined. In this study, the
85 dominant aqSOA precursor is GUA (Henry's law constant of $9.2 \times 10^2 \text{ M atm}^{-1}$; Sagebiel et al., 1992), and DMB and VL
86 were used as photosensitizers to oxidize GUA. DMB and VL (Henry's law constants of $7.3 \times 10^3 \text{ M atm}^{-1}$ and $4.7 \times 10^5 \text{ M}$
87 atm^{-1} , respectively; Yaws, 1994; EPI Suite version 4.1, 2012; Felber et al., 2021), which are also abundant in BB emissions
88 (Schauer et al., 2001; Li et al., 2014; Chen et al., 2017; Pang et al., 2019; Mabato et al., 2022) and whose structures differ
89 only by one functional group ($-\text{OCH}_3$ for the former and $-\text{OH}$ for the latter, Fig. 1), represented non-phenolic and phenolic
90 methoxybenzaldehydes, respectively. The structures of GUA, DMB, and VL are provided in Figure 1. Based on their
91 quantum yield of $^3\text{C}^*$ formation, DMB and VL have been classified as moderate and poor photosensitizers, respectively
92 (Felber et al., 2021). The photosensitized oxidation of GUA by $^3\text{DMB}^*$ or $^3\text{VL}^*$ in the absence (and presence) of AN are
93 referred to as GUA+DMB(+AN) and GUA+VL(+AN), respectively. GUA photo-oxidation by AN alone (GUA+AN) was
94 also explored for comparison with GUA+DMB+AN and GUA+VL+AN. The molar absorptivities of GUA, DMB, VL, and
95 nitrate are shown in Figure 1. The precursor and photosensitizer decay kinetics, detected products, and absorbance
96 enhancement were used to characterize the reactions. However, it should be noted that we mainly focused on the analyses of
97 the reaction products and product distribution.

98 While several studies on photo-oxidation of BB emissions are available, this work focuses on the comparison
99 between non-phenolic and phenolic methoxybenzaldehydes as photosensitizers in the absence and presence of AN for
100 aqSOA formation. We found that GUA oxidation by $^3\text{DMB}^*$ was faster and exhibited greater light absorption relative to
101 GUA+VL. These are likely attributed to the stronger photosensitizing ability of DMB and the $-\text{OH}$ group of VL, making it
102 more prone to oxidation and more reactive towards electrophilic aromatic substitution. Oligomerization and functionalization
103 dominated in GUA+DMB and GUA+VL, but functionalization appeared to be more significant in GUA+VL due to VL
104 transformation products. Although AN did not significantly influence the oxidation kinetics due to the predominant role of
105 photosensitizer chemistry compared to nitrate, AN promoted the formation of N-containing products. These include N-
106 heterocycles (e.g., imidazoles), suggesting the participation of ammonium in the reactions. Moreover, the product
107 distributions indicate distinct interactions between photosensitization by $^3\text{DMB}^*$ and $^3\text{VL}^*$ and AN photolysis. In particular,
108 AN generated more N-containing products in GUA+DMB+AN than in GUA+VL+AN, and increased the oligomers in
109 GUA+VL+AN. Furthermore, increased nitrated compounds in GUA+DMB+AN and GUA+VL+AN compared to GUA+AN
110 suggest that photosensitized reactions may promote reactions by nitrate photolysis.

111 **2 Methods**

112 **2.1 Aqueous phase photo-oxidation experiments**

113 Procedures for the photo-oxidation experiments are presented in detail in our previous study (Mabato et al., 2022).
114 Experimental solutions were prepared using 0.1 mM guaiacol (GUA, Sigma Aldrich, $\geq 98.0\%$) and 0.01 mM 3,4-
115 dimethoxybenzaldehyde (DMB, Acros Organics, 99+%) or 0.01 mM vanillin (VL, Acros Organics, 99%, pure), in the
116 absence and presence of ammonium nitrate (1 mM; AN, Acros Organics, 99+%, for analysis). These GUA and
117 methoxybenzaldehydes concentrations are within the values expected in cloud or fog drops in areas with significant wood
118 combustion (Anastasio et al., 1997; Rogge et al., 1998; Nolte et al., 2001). The AN concentration represents values usually
119 observed in cloud and fog waters (Munger et al., 1983; Collett et al., 1998; Zhang and Anastasio, 2003; Li et al., 2011;
120 Giulianelli et al., 2014; Bianco et al., 2020). It must be noted that this study did not intend to identify the AN concentrations
121 that would affect the kinetics but attempted to analyze the effects of AN on photosensitized aqSOA formation. A solution
122 composed of 0.1 mM GUA and 1 mM AN (GUA+AN) was also examined for comparison with GUA+DMB+AN and
123 GUA+VL+AN. Sulfuric acid (H_2SO_4 ; Acros Organics, ACS reagent, 95% solution in water) was used to adjust the pH of the
124 solutions to 4, which is within typical cloud pH values (2–7; Pye et al., 2020) and pH values observed in wood burning-
125 impacted cloud and fog waters (Collett et al., 1998; Raja et al., 2008). The solutions (initial volume of 500 mL) were
126 bubbled with synthetic air (0.5 dm^3/min) for 30 min before irradiation and throughout the reactions to achieve air-saturated
127 conditions (Du et al., 2011; Chen et al., 2020) and were continuously magnetically stirred. In this study, the reactions can
128 generate $^3\text{DMB}^*/^3\text{VL}^*$ and secondary oxidants ($^1\text{O}_2$, $\text{O}_2^{\cdot-}/\text{HO}_2$, $^{\cdot}\text{OH}$) but not ozone. Solutions contained in a quartz
129 photoreactor were irradiated using a xenon lamp (model 6258, Ozone free xenon lamp, 300 W, Newport) equipped with a

130 longpass filter (20CGA-305 nm cut-on filter, Newport) to eliminate light below 300 nm. The reaction temperatures were
131 maintained at 27 ± 2 °C using cooling fans positioned around the photoreactor and lamp housing. The averaged initial
132 photon flux in the reactor measured from 300 to 380 nm was $\sim 3 \times 10^{15}$ photons $\text{cm}^{-2} \text{s}^{-1} \text{nm}^{-1}$ (Fig. 1), similar to our previous
133 work (Mabato et al., 2022). Samples were collected every 30 min for 180 min for offline analyses of (1) GUA, DMB, and
134 VL concentrations using ultra-high-performance liquid chromatography with photodiode array detector (UHPLC-PDA) and
135 (2) absorbance measurements using UV-Vis spectrophotometry. Moreover, the samples collected before and after irradiation
136 (180 min) were analyzed for (3) reaction products using UHPLC coupled with heated electrospray ionization Orbitrap mass
137 spectrometry (UHPLC-HESI-Orbitrap-MS) operated in positive and negative ion modes and (4) concentrations of small
138 organic acids using ion chromatography (IC). Each experiment was repeated independently at least three times. The reported
139 decay rate constants, small organic acids concentration, and absorbance enhancement were averaged from triplicate
140 experiments, and the corresponding errors represent one standard deviation. The pseudo-first-order rate constant (k') for
141 GUA decay was determined using the following equation (Huang et al., 2018):

$$142 \quad \ln ([\text{GUA}]_t / [\text{GUA}]_0) = -k't \quad (\text{Eq. 1})$$

143 where $[\text{GUA}]_t$ and $[\text{GUA}]_0$ are GUA concentrations at time t and 0, respectively. DMB or VL decay rate constants were
144 calculated by replacing GUA with DMB or VL in Eq. 1. The decay rate constants were normalized to the photon flux
145 measured for each experiment through dividing k' by the measured 2-nitrobenzaldehyde (2NB; a chemical actinometer)
146 decay rate constant, $j(2\text{NB})$ (Mabato et al., 2022). In addition, the decay rate constants were corrected for the internal light
147 screening due to DMB, VL, and AN (Leifer, 1988; Zhang and Anastasio, 2003; Smith et al., 2014, 2016). The values of the
148 internal light screening factor (S_i) determined around the peak in the light absorption action spectrum (DMB: 310-335 nm,
149 VL: 304-364 nm, nitrate: 300-331 nm) (Smith et al., 2014, 2016) for an 8.5 cm cell were 0.95 for GUA+AN, 0.51 for
150 GUA+DMB, 0.54 for GUA+DMB+AN, 0.57 for GUA+VL, and 0.59 for GUA+VL+AN. Moreover, two independently
151 prepared samples for each reaction condition were analyzed using UHPLC-HESI-Orbitrap-MS. Only peaks that were
152 reproducibly detected in both sets of samples were considered. For clarity, the formulas discussed in this work correspond to
153 neutral analytes (e.g., with H^+ or NH_4^+ removed from the ion formula). The details of the analytical procedures are provided
154 in the Supplement (Sects. S1 to S4).

155 **2.2 Calculation of normalized abundance of products**

156 Several recent studies have used comparisons of relative abundance of products based on peak areas from mass spectrometry
157 (MS) results (e.g., Lee et al., 2014; Romonosky et al., 2017; Wang et al., 2017; Fleming et al., 2018; Song et al., 2018; Klodt
158 et al., 2019; Ning et al., 2019) to show the relative importance of different types of compounds (K. Wang et al., 2021).
159 However, comparisons of relative abundance among different compounds can be subject to uncertainties as ionization
160 efficiencies in soft ionization, such as ESI, may significantly vary between different compounds (Kearle, 2000; Schmidt et
161 al., 2006; Leito et al., 2008; Perry et al., 2008; Krue et al., 2014). In our previous work (Mabato et al., 2022), we introduced
162 the normalized abundance of products ($[\text{P}]$, unitless) (Eq. 2) as a semi-quantitative analysis that gives an overview of how

163 the signal intensities changed under different experimental conditions but not the quantification of the absolute product
164 concentration. The calculation assumes equal ionization efficiencies of different compounds, which is commonly used to
165 estimate O:C ratios of SOA (Bateman et al., 2012; Lin et al., 2012; Laskin et al., 2014; De Haan et al., 2019):

166

$$167 \quad [P] = \frac{A_{P,t}}{A_{GUA,t}} \cdot \frac{[GUA]_t}{[GUA]_0} \quad (\text{Eq. 2})$$

168 where $A_{P,t}$ and $A_{GUA,t}$ are the extracted ion chromatogram (EIC) peak areas of the product P and GUA from UHPLC-HESI-
169 Orbitrap-MS analyses at time t , respectively; $[GUA]_t$ and $[GUA]_0$ are the GUA concentrations (μM) determined using
170 UHPLC-PDA at time t and 0, respectively. Note that the normalized abundance of products has intrinsic uncertainties due to
171 the variability in ionization efficiencies for various compounds. Moreover, it should be noted that the normalized abundance
172 of products was calculated using only the positive ion mode data as the GUA signal from the negative ion mode was weak
173 and thus may present large uncertainties during normalization. Therefore, products that may not give signals or may have
174 weak signals in the positive ion mode were possibly underestimated in the normalized product abundance. Nevertheless, it
175 enables the comparison of MS results among different experiments. As demonstrated in our previous work (Mabato et al.,
176 2022) and the current study, a higher normalized abundance of products generally correlates with higher efficiency of
177 oxidation. The reported uncertainties were propagated from the changes in $[GUA]$ measured using UHPLC-PDA and the MS
178 signal intensities.

179

180 **3 Results and Discussion**

181 Using kinetics data, MS analyses, and absorbance enhancement data, we first examined the differences between GUA+DMB
182 and GUA+VL (Sect. 3.1). Then, we analyzed GUA+DMB+AN, GUA+VL+AN, and GUA+AN (Sect. 3.2) to explore the
183 effects of nitrate photolysis and ammonium on photosensitized aqSOA formation.

184 **3.1 Comparison of photosensitized GUA oxidation by non-phenolic ($^3\text{DMB}^*$) and phenolic ($^3\text{VL}^*$)** 185 **methoxybenzaldehydes**

186 Prior studies have reported that photosensitized non-carbonyl phenol oxidation in the presence of 3,4-
187 dimethoxybenzaldehyde (DMB) and vanillin (VL) (separately) was mainly driven by $^3\text{DMB}^*$ and $^3\text{VL}^*$, respectively (Smith
188 et al., 2014; Mabato et al., 2022), while contributions from secondary oxidants such as $^1\text{O}_2$ and $^{\bullet}\text{OH}$ were likely minor.
189 However, both $^3\text{DMB}^*$ and $^3\text{VL}^*$ are efficiently quenched by O_2 , suggesting that energy transfer should be considered in
190 evaluating photosensitized processes involving these methoxybenzaldehydes (Felber et al., 2021). Moreover, it was found
191 that $^3\text{DMB}^*$, $^1\text{O}_2$, and $\text{O}_2^{\bullet-}$ were the major contributors to the photosensitized oxidation of 4-ethylguaiaicol (Chen et al., 2020).
192 Recently, the oxidation of guaiacyl acetone (a non-conjugated phenolic carbonyl) in the presence of DMB has been reported

193 to be initiated by $^3\text{DMB}^*$, $^1\text{O}_2$, $^{\bullet}\text{OH}$, or methoxy radical ($^{\bullet}\text{OCH}_3$) (Misovich et al., 2021). Further studies are thus required to
194 identify the specific oxidants in these reaction systems. In this study, reactions initiated in the presence of DMB or VL are
195 collectively referred to as photosensitized reactions. The reaction conditions, initial guaiacol (GUA) and DMB or VL decay
196 rate constants, normalized product abundance, and the chemical characteristics of aqSOA formed in this work are
197 summarized in Table 1.

198 **3.1.1 Kinetic analysis of photosensitization by $^3\text{DMB}^*$ and $^3\text{VL}^*$**

199 No significant loss of GUA or photosensitizers was observed for dark experiments ($p > 0.05$). Figure S1 shows the decay of
200 GUA, DMB, and VL under different experimental conditions. Upon irradiation, the GUA decay rate constant in GUA+DMB
201 was ~4 times higher than in GUA+VL. In GUA+DMB, the decay rate constant of GUA was ~8 times higher than that of
202 DMB, consistent with a previous study (Smith et al., 2014). Contrastingly, the decay rate constant of VL was 2.4 times
203 higher than that of GUA in GUA+VL. This VL consumption was also observed in our earlier work using 0.1 mM GUA +
204 0.1 mM VL (Mabato et al., 2022). These trends could be explained by the following reasons. First, DMB has a stronger
205 photosensitizing ability than VL based on its higher quantum yield of $^3\text{C}^*$ formation and longer lifetime of $^3\text{DMB}^*$
206 compared to $^3\text{VL}^*$ (Felber et al., 2021). Second, VL is also a phenolic compound similar to GUA, and is therefore highly
207 reactive towards oxidation. For instance, its $-\text{OH}$ group can be oxidized by $^3\text{VL}^*$ via H-atom abstraction to form phenoxy
208 radicals which can undergo coupling to form oligomers (Kobayashi and Higashimura, 2003; Sun et al., 2010; Mabato et al.,
209 2022). The faster consumption of VL than GUA suggests a competition between ground-state VL and GUA for reaction with
210 $^3\text{VL}^*$. Moreover, compared to a $-\text{OCH}_3$ group (in DMB), an $-\text{OH}$ group (in VL) has a stronger electron-donating ability and
211 is thus more activating towards electrophilic aromatic substitution. It should be noted that the differences in the GUA decay
212 rate constants among different reaction systems are not quantitatively equivalent to photosensitizing efficiencies, and a
213 detailed quantitative analysis of which is beyond the scope of this study. Nonetheless, these results suggested that GUA
214 oxidation in GUA+DMB was overall more efficient than in GUA+VL. Our kinetic analysis focused on the decay rate
215 constants of the aqSOA precursor (GUA) and the photosensitizers (DMB and VL) during photosensitization under the same
216 experimental conditions (same aqSOA precursor and concentration, same photosensitizer concentration, and same lamp
217 photon flux). The effects of other factors (e.g., intersystem crossing efficiency) on the rate constants were not examined.
218 Explicit kinetic studies (e.g., Smith et al., 2014, 2015) that measure second-order rate constants should be conducted in the
219 future to extend the applicability of the kinetic parameters to other conditions.

220 **3.1.2 Product distributions and chemical characteristics of aqSOA from photosensitization by $^3\text{DMB}^*$ and $^3\text{VL}^*$**

221 The products detected using UHPLC-HESI-Orbitrap-MS were used to characterize the aqSOA formed in this work. The
222 signal-weighted distributions of aqSOA calculated from combined positive (POS) and negative (NEG) ion modes MS results
223 are summarized in Figure 2. The signal-weighted distributions calculated separately from POS and NEG ion modes MS
224 results are available in Figures S2 and S3. It should be noted that in this work, the product distributions for all experiments

225 were based on the same irradiation time of 180 min. An irradiation time of 180 min was chosen as it was sufficient to show
226 the differences in the extent of reaction of GUA among the reaction systems studied. For reaction systems with precursors of
227 different reactivities, chemical analysis at a fixed reaction time may be looking at different generations of products of each
228 precursor, as Yu et al. (2014) reported. Measuring the product distribution at a fixed time might have missed the information
229 on what/how many products are formed at the similar amounts of precursors reacted. The situation could be even more
230 complicated if different precursors had major differences in pathways and dominant intermediates. However, comparing the
231 product distributions after a certain time of light exposure, as is the case for this study, is useful to evaluate what products
232 would form after a certain time of photosensitization. Oligomers and derivatives of GUA dominated both GUA+DMB and
233 GUA+VL, in agreement with pronounced oligomerization from triplet-mediated oxidation of relatively high phenol
234 concentration (e.g., 0.1 to 3 mM; Li et al., 2014; Yu et al., 2014, 2016; Slikboer et al., 2015; Ye et al., 2019; Mabato et al.,
235 2022). Figure 3 schematically depicts the main differences between photosensitized GUA oxidation by $^3\text{DMB}^*$ and $^3\text{VL}^*$ in
236 the absence and presence of AN. As shown in Fig. 3, $^3\text{DMB}^*$ and $^3\text{VL}^*$ can oxidize GUA via H-atom abstraction to form
237 phenoxy radicals which undergo coupling to form oligomers (Kobayashi and Higashimura, 2003; Sun et al., 2010; Mabato et
238 al., 2022). The higher oligomer contribution in GUA+DMB is likely due to the better photosensitizing ability of DMB than
239 VL and partly the lower abundance of $^3\text{VL}^*$ due to fast VL consumption. VL was consumed faster than DMB during GUA
240 oxidation ascribable to the $-\text{OH}$ group of VL, making it more susceptible to oxidation and more reactive towards
241 electrophilic aromatic substitution. In addition, the normalized product abundance for GUA+DMB was ~ 4 times higher than
242 that for GUA+VL (Table 1), further suggesting more efficient photosensitized GUA oxidation by $^3\text{DMB}^*$ than by $^3\text{VL}^*$. The
243 oxidation of GUA or transient organic intermediates by secondary oxidants (e.g., $^1\text{O}_2$ and $\cdot\text{OH}$) from $^3\text{DMB}^*$ or $^3\text{VL}^*$ and the
244 fragmentation of larger compounds generate highly oxidized ring-opening products (Yu et al., 2014; Huang et al., 2018;
245 Chen et al., 2020). GUA+DMB had a higher contribution of ring-opening products than GUA+VL, likely due to the greater
246 availability of secondary oxidants in the former and fast VL consumption lowering the production of these species in
247 GUA+VL. The IC analyses also indicate the formation of small organic acids (e.g., formic acid), which appeared to have
248 higher concentrations in the presence of DMB than in VL (Fig. S4). Although no data is available for the concentration
249 changes (every 30 min) of small organic acids during the reaction, it is likely that an increasing trend would be observed as
250 fragmentation, which leads to the decomposition of initially formed oligomers and the generation of smaller oxygenated
251 products, becomes important at longer irradiation times (Huang et al., 2018). This trend has also been observed in our
252 previous work on the direct photosensitized oxidation of VL (Mabato et al., 2022), as well as other studies on
253 photosensitized oxidation of non-carbonyl phenols and phenolic carbonyls (e.g., Yu et al., 2016; Jiang et al., 2021). The
254 reactions of secondary oxidants or ring-opening products with GUA can form functionalized products. Notably, the
255 contribution of monomers in GUA+VL was almost twice as high as in GUA+DMB, ascribable to VL transformation
256 products. We previously showed that for the direct photosensitized oxidation of VL, functionalization prevails over
257 oligomerization at 0.01 mM VL, the [VL] used in this work, while oligomerization dominates at higher [VL] (0.1 mM;
258 Mabato et al., 2022).

259 It has been reported that oligomerization could occur during the electrospray ionization process (Yasmeen et al.,
260 2010). In this work, it was confirmed that the oligomers observed were generated in the solutions via aqueous reactions
261 instead of being artefacts of HESI-MS. This is based on the absence of dimers and higher oligomers in the HESI mass
262 spectra of dark control solutions acquired by direct infusion (Yu et al., 2016).

263 The major GUA+DMB and GUA+VL products (Tables S1-S2) are mostly oligomers which can be formed through
264 the coupling of phenoxy radicals (Kobayashi and Higashimura, 2003; Sun et al., 2010; Mabato et al., 2022). GUA+DMB
265 products matched those reported in previous works on ³DMB*- and/or -OH-mediated phenol oxidation (Yu et al., 2014,
266 2016). These include GUA dimers and trimers (e.g., C₁₄H₁₄O₄ and C₂₁H₁₈O₈, #1 and 19; Table S1), aldehydes (C₇H₆O₄, #13;
267 Table S1), and esters (C₁₆H₁₈O₆, #14; Table S1). Functionalized products include C₁₁H₁₂O₅ and C₁₀H₁₂O₃ (#8 and 12; Table
268 S1). More than half of the major GUA+VL products are the same oligomers detected from GUA+DMB (e.g., C₁₃H₁₀O₄ and
269 C₂₀H₁₈O₆, #4 and 21; Table S1). The rest are mainly functionalized species such as C₇H₈O₄ and C₈H₈O₅ (#28 and 35; Table
270 S2), corresponding to a hydroxylated GUA and hydroxylated VL, respectively.

271 The average elemental ratios and elemental distribution of the products (Fig. S5a–d) were consistent with those in
272 previous studies on similar reaction systems (Yu et al., 2014, 2016; Mabato et al., 2022). The majority of the GUA+DMB
273 and GUA+VL products had H:C ≤1.0 and O:C ≤0.5, typical for aromatic species (Mazzoleni et al., 2012; Kourtchev et al.,
274 2014; Jiang et al., 2021). GUA+DMB had more compounds with higher O:C (≥0.6), in agreement with higher contributions
275 of ring-opening products than in GUA+VL (Fig. 2). The higher ⟨OS_C⟩ for GUA+VL than in GUA+DMB (Table 1) was
276 probably due to the significant functionalization in the former. Moreover, the distributions of OS_C and carbon number (Fig.
277 S6a–d) show that these aqSOA products have similar elemental composition to those of low-volatility oxygenated organic
278 aerosols (LV-OOA), semi-volatile oxygenated organic aerosols (SV-OOA), and slightly with biomass burning organic
279 aerosols (BBOA) (Kroll et al., 2011). Further discussions on van Krevelen diagrams (Fig. S5a–d) and OS_C vs. carbon
280 number plots (Fig. S6a–d) for GUA+DMB and GUA+VL aqSOA are available in the Supplement (Sect. S5). In brief,
281 ³DMB*-initiated GUA oxidation was faster and yielded higher normalized product abundance than oxidation by ³VL*. This
282 is likely due to the stronger photosensitizing ability of DMB than VL and the -OH group of VL facilitating its rapid
283 consumption. In addition, oligomerization and functionalization dominated in both GUA+DMB and GUA+VL, as reported
284 in similar studies (Yu et al., 2014, 2016; Chen et al., 2020; Jiang et al., 2021; Misovich et al., 2021; Mabato et al., 2022).
285 However, functionalization was more prominent in the latter, attributable to the transformation of VL. Nonetheless, it must
286 be noted that for phenolic aqSOA, fragmentation will ultimately be more predominant at longer irradiation times (Huang et
287 al., 2018; Yu et al., 2016; Mabato et al., 2022).

288 3.1.3 Light absorption of aqSOA from photosensitization by ³DMB* and ³VL*

289 The absorbance enhancement of phenolic aqSOA generated via reactions with ³DMB*/³VL* has been linked to the
290 formation of conjugated structures due to oligomerization and functionalization (e.g., additions of hydroxyl and carbonyl
291 groups; Yu et al., 2014, 2016; Smith et al., 2016; Chen et al., 2020; Jiang et al., 2021; Misovich et al., 2021; Mabato et al.,

292 2022). Moreover, the aqueous-phase photo-oxidation of BB emissions can enhance BrC absorbance via the formation of
293 aromatic dimers and functionalized products (Hems et al., 2020). The increase in light absorption throughout 180 min of
294 irradiation and the change in the rate of sunlight absorption (ΔR_{abs}) (Jiang et al., 2021) from 350 to 550 nm at 180 min during
295 typical clear and haze days in Beijing, China for all the reaction systems studied are provided in Figure 4. Figure S7 shows
296 the absorption spectra after 180 min of irradiation for each reaction system studied. In this work, the absorbance
297 enhancement of GUA+DMB and GUA+VL (Fig. 4a) could be due to oligomers and functionalized monomers, which are the
298 highest contributors to the product signals. Identifying the chromophores responsible for the absorbance enhancement may
299 be beneficial in understanding the impact of aqSOA on the Earth's radiative balance and determining the reactions that affect
300 light absorption by aqSOA (Mabato et al., 2022). However, the detected products did not exhibit distinct peaks in the
301 UHPLC-PDA chromatograms, likely due to the concentration of the chromophores being below the detection limit of PDA.
302 Nevertheless, the higher absorbance enhancement and ΔR_{abs} for GUA+DMB than GUA+VL was probably due to the higher
303 contribution and normalized abundance (by ~6 times) of oligomers in the former.

304 Additional information about aqSOA light absorption can be deduced from the plots of the double bond equivalent
305 (DBE) values vs. carbon number (n_C) (Lin et al., 2018). Figure S8 shows these plots along with the DBE reference values of
306 fullerene-like hydrocarbons (Lobodin et al., 2012), cata-condensed polycyclic aromatic hydrocarbons (PAHs; Siegmann and
307 Sattler, 2000), and linear conjugated polyenes with a general formula C_xH_{x+2} . The shaded area indicates a sufficient level of
308 conjugation for visible light absorption, and species within this region are potential BrC chromophores. GUA+DMB and
309 GUA+VL aqSOA exhibited a significant overlap in the DBE vs. n_C space; nearly all products from both systems, including
310 the high-relative-abundance species, are potential BrC chromophores. GUA+DMB had more oligomeric products with high
311 relative abundance ($n_C \geq 12$ and $\text{DBE} \geq 8$). For GUA+VL, high-relative-abundance products also include monomeric species
312 ($n_C = 7-8$ and 4-5 DBE) corresponding to hydroxylated products (e.g., $C_7H_8O_4$ and $C_8H_8O_5$; 28 and 35; Table S2). These
313 observations further indicate the importance of oligomerization and functionalization for the absorbance enhancement of
314 aqSOA generated via photosensitization by $^3\text{DMB}^*$ and $^3\text{VL}^*$. In summary, $^3\text{DMB}^*$ and $^3\text{VL}^*$ can oxidize GUA resulting in
315 aqSOA and BrC formation, but GUA+DMB products exhibited stronger light absorption. In GUA+VL, the extent of GUA
316 oxidation was limited by significant VL consumption.

317 **3.2 Comparison of photosensitized GUA oxidation by non-phenolic ($^3\text{DMB}^*$) and phenolic ($^3\text{VL}^*$)** 318 **methoxybenzaldehydes in the presence of AN**

319 **3.2.1 Kinetic analysis of photosensitization by $^3\text{DMB}^*$ and $^3\text{VL}^*$ in the presence of AN**

320 Ammonium nitrate (AN) did not significantly affect ($p > 0.05$) the decay rate constants of GUA, DMB, and VL for both
321 GUA+DMB+AN and GUA+VL+AN (Table 1), likely due to the higher molar absorptivities of the photosensitizers
322 compared to that of nitrate. This implies that the chemistry of $^3\text{DMB}^*$ and $^3\text{VL}^*$ dominated that of nitrate. In this work, the
323 GUA decay rate constants decreased in the order of GUA+DMB/GUA+DMB+AN > GUA+VL/GUA+VL+AN > GUA+AN
324 (Table 1). Note that as the molar absorptivities of the photosensitizers are higher than that of nitrate, the kinetics data were

325 also analyzed on a per-photon-absorbed basis for a more appropriate comparison of reaction efficiency (Sect. S6). The
326 apparent quantum efficiency of GUA photodegradation (ϕ_{GUA}) in the presence of nitrate (GUA+AN: $0.17 \pm 3.8 \times 10^{-2}$) was
327 ~ 2 and ~ 7 times higher than that in the presence of DMB ($0.10 \pm 2.9 \times 10^{-3}$) or VL ($0.026 \pm 7.2 \times 10^{-3}$), respectively. This
328 suggests that nitrate-mediated GUA photo-oxidation is more efficient than photosensitization by $^3\text{DMB}^*$ or $^3\text{VL}^*$ on a per-
329 photon-absorbed basis.

330 **3.2.2 Product distributions and chemical characteristics of aqSOA from photosensitization by $^3\text{DMB}^*$ and $^3\text{VL}^*$ in** 331 **the presence of AN**

332 For both GUA+DMB+AN and GUA+VL+AN, AN had no significant effect on the normalized product abundance (Table 1),
333 but it induced the formation of N-containing products composed of N-heterocycles (e.g., imidazoles and pyridines) and
334 oligomers, as well as nitrated species. Similarly, we previously reported a potential imidazole derivative from the direct
335 photosensitized oxidation of VL in the presence of AN, which was attributed to the reaction of ring-opening products with
336 dissolved ammonia (Mabato et al., 2022). Oligomers remained the highest signal contributors in the presence of AN (Fig. 2),
337 but interactions between photosensitization by $^3\text{DMB}^*$ and $^3\text{VL}^*$ and AN photolysis were distinct. First, nitrated species had
338 similar contributions in both cases, but the contribution and normalized abundance of all N-containing products in
339 GUA+DMB+AN were 2 and ~ 14 times higher, respectively, than in GUA+VL+AN. This difference can be attributed to the
340 higher contribution of N-heterocycles and N-containing oligomers in GUA+DMB+AN. Compared to GUA+VL,
341 GUA+DMB had a higher contribution of ring-opening products which can react with ammonia, as discussed earlier (Figs. 2
342 and 3). Second, the decrease in oligomers in GUA+DMB+AN may be due to their fragmentation induced by $\cdot\text{OH}$ from
343 nitrate photolysis, then conversion to N-containing products. Correspondingly, the contribution of possibly ring-retaining N-
344 containing products in GUA+DMB+AN (18.6%) was ~ 3 times higher than that in GUA+VL+AN (6.5%). While
345 fragmentation of oligomers likely occurred in GUA+VL+AN as well, the increase in oligomers suggests that other reactions
346 have taken place. For GUA+VL+AN, $\cdot\text{OH}$ or $\cdot\text{NO}_2$ from nitrate photolysis may have initiated H-atom abstraction from the –
347 OH group of VL, generating phenoxy radicals which can undergo coupling to form more oligomers (Kobayashi and
348 Higashimura, 2003; Sun et al., 2010; Mabato et al., 2022). This may also explain the more significant decrease of monomers
349 in GUA+VL+AN (~ 3 times) compared to GUA+DMB+AN (~ 2 times). Similarly, we previously observed an increase in
350 oligomers during the direct photosensitized oxidation of 0.01 mM VL (Mabato et al., 2022), the [VL] used in this work,
351 upon adding 1 mM AN. These findings indicate that photosensitization by non-phenolic and phenolic
352 methoxybenzaldehydes may interact differently with AN photolysis.

353 GUA+AN mainly formed oligomers analogous to $\cdot\text{OH}$ -mediated phenol oxidation (Yu et al., 2014, 2016), followed
354 by N-containing products. The normalized product abundance of GUA+AN was the lowest among all experiments, likely
355 due to the lower GUA decay constant relative to photosensitized oxidation. Moreover, the normalized abundance of N-
356 containing products in GUA+AN was ~ 12 times lower than that in GUA+DMB+AN but comparable to that in
357 GUA+VL+AN. This discrepancy for GUA+VL+AN might be due to the weaker signals of its N-containing products in the

358 positive compared to the negative ion mode. As previously mentioned, the normalized product abundance was calculated
359 using only the positive ion mode data as the GUA signal from the negative ion mode was weak and thus may present large
360 uncertainties during normalization. Interestingly, the contributions from nitrated species in GUA+DMB+AN and
361 GUA+VL+AN were higher than in GUA+AN, suggesting possible enhancement of nitration reactions. This is likely due to
362 the increased formation of $\cdot\text{NO}_2$, for instance, via the reactions of $\cdot\text{OH}$ and $\text{O}_2\cdot^-$ (from $^3\text{DMB}^*$ or $^3\text{VL}^*$) with NO_2^- (Pang et
363 al., 2019; Mabato et al., 2022). Similarly, we previously reported enhanced nitration via the direct photosensitized oxidation
364 of VL in the presence of AN under air-saturated conditions (O_2 is present) relative to nitrogen-saturated conditions (Mabato
365 et al., 2022). These imply that photosensitization may promote reactions induced by nitrate photolysis.

366 The major products from GUA+DMB+AN, GUA+VL+AN, and GUA+AN (Tables S3–S5) include oligomers and
367 functionalized monomers detected in GUA+DMB and GUA+VL (Tables S1–S2). The N-heterocycles from
368 GUA+DMB+AN include $\text{C}_6\text{H}_6\text{N}_4$ (#41; Table S3), which may be 2,2'-biimidazole (BI), a reaction product from glyoxal +
369 reduced nitrogenous compounds (e.g., ammonium salts) (De Haan et al., 2009; Galloway et al., 2009; Nozière et al., 2009;
370 Shapiro et al., 2009; Yu et al., 2011; Kampf et al., 2012; Gen et al., 2018; Mabato et al., 2019). The nitrated products include
371 $\text{C}_{12}\text{H}_{11}\text{N}_3\text{O}_3$ and $\text{C}_{15}\text{H}_{10}\text{N}_4\text{O}_3$ (#42 and 49; Table S3), which possibly have a nitrated imidazole moiety and a nitrophenol
372 moiety, respectively. For GUA+VL+AN, oligomers ($\text{C}_{14}\text{H}_{12}\text{O}_6$ and $\text{C}_{20}\text{H}_{16}\text{O}_7$; #55 and 59, Table S4) which were not among
373 the major products in GUA+VL were noted. $\text{C}_{10}\text{H}_8\text{O}_2$ likely has a furanone group (#50; Table S4); furanones are the primary
374 products of the reaction of $\cdot\text{OH}$ with toluene and other aromatic hydrocarbons (Smith et al., 1999). Moreover, $\text{C}_{11}\text{H}_9\text{N}_3\text{O}_3$
375 (#57; Table S4) has a nitrated imidazole moiety. Among the N-containing compounds in GUA+AN is $\text{C}_4\text{H}_3\text{N}_3\text{O}_3$ (#69; Table
376 S5), which may be a nitrated imidazole-2-carboxaldehyde. Imidazole-2-carboxaldehyde is also a reaction product from
377 glyoxal + reduced nitrogenous compounds (e.g., ammonium salts) (De Haan et al., 2009; Galloway et al., 2009; Nozière et
378 al., 2009; Shapiro et al., 2009; Yu et al., 2011; Kampf et al., 2012; Gen et al., 2018; Mabato et al., 2019).

379 The $\langle\text{O:C}\rangle$ for GUA+DMB+AN and GUA+VL+AN were lower than those in the absence of AN (Table 1), possibly
380 due to the formation of N-heterocycles, altering the elemental ratios. The $\langle\text{O:C}\rangle$ and $\langle\text{H:C}\rangle$ were comparable in
381 GUA+DMB+AN and GUA+VL+AN, but the $\langle\text{N:C}\rangle$ for the former was higher, implying a greater extent of reactions
382 involving AN. Relative to GUA+DMB+AN and GUA+VL+AN, GUA+AN had a higher $\langle\text{N:C}\rangle$, as can be expected given
383 that AN was the only oxidant source. The lower $\langle\text{OS}_\text{C}\rangle$ of GUA+DMB+AN and GUA+VL+AN compared to GUA+AN may
384 be attributed to triplet-initiated oxidation generating higher-molecular-weight products with less fragmentation compared to
385 $\cdot\text{OH}$ -mediated oxidation (Yu et al., 2014; Chen et al., 2020). Nonetheless, AN generally increased the $\langle\text{OS}_\text{C}\rangle$ for both
386 GUA+DMB and GUA+VL, with a more noticeable increase for the former, suggesting more oxidized products. Similarly, in
387 a previous work, the more oxygenated and oxidized aqSOA from the photo-oxidation of phenolic carbonyls in AN solutions
388 than in ammonium sulfate solutions has been ascribed to nitrate photolytic products promoting the reactions (Huang et al.,
389 2018). Furthermore, GUA+DMB+AN and GUA+VL+AN aqSOA had mainly similar features in the OS_C vs. n_C plots as
390 those observed in the absence of AN (Fig. S6). More information on van Krevelen diagrams (Figs. S5e–h and S9) and OS_C
391 vs. n_C plots (Figs. S6e–h and S10) for GUA+DMB+AN, GUA+VL+AN, and GUA+AN aqSOA are provided in the

392 Supplement (Sect. S7). In essence, AN had no significant effect on the decay kinetics ascribable to photosensitizer chemistry
393 prevailing over nitrate, but it induced the formation of N-containing products. Moreover, AN modified the product
394 distributions, albeit in different ways (Figs. 2 and 3). In particular, N-containing products were more abundant in
395 GUA+DMB+AN, probably due to more extensive fragmentation in GUA+DMB than in GUA+VL. In GUA+VL+AN, AN
396 promoted oligomer formation likely via the -OH group of VL. Furthermore, GUA+DMB+AN and GUA+VL+AN had more
397 nitrated products than GUA+AN, suggesting that photosensitized reactions may promote nitrate photolysis-initiated
398 reactions.

399 **3.2.3 Light absorption of aqSOA from photosensitization by ³DMB* and ³VL* in the presence of AN**

400 The presence of AN also did not appreciably affect the absorbance enhancement and ΔR_{abs} for both GUA+DMB+AN and
401 GUA+VL+AN (Fig. 4). For GUA+DMB+AN, the N-containing products may have offset the decrease in oligomers to
402 maintain the absorbance enhancement observed from GUA+DMB. Wang et al. (2022) reported that nitration might
403 contribute significantly to absorbance enhancement for methoxyphenols in sodium nitrate. In GUA+VL+AN, the decrease in
404 monomers may have counteracted the increased oligomers and the generated N-containing products. Compared to
405 GUA+DMB+AN, the N-containing products from GUA+VL+AN probably had less impact on the absorbance enhancement
406 based on their smaller signal contribution.

407 Similar to experiments without AN, CHO species from GUA+DMB+AN and GUA+VL+AN were mainly
408 overlapped in the DBE vs. n_c space (Fig. S8c,d) and were mostly potential BrC chromophores. In both systems, GUA dimers
409 were the products with the highest relative abundance. For GUA+DMB+AN, products with high relative abundance also
410 include a CHN species, while two CHON species had high n_c (18,20) and DBE (16,14) values. In GUA+VL+AN, products
411 with high relative abundance include a CHON species ($n_c = 11$ and 9 DBE). Approximately 30% and 43% of the N-
412 containing products for GUA+DMB+AN and GUA+VL+AN, respectively, were among the potential BrC chromophores.
413 This suggests the possible significance of N-containing products for light absorption of aqSOA from photosensitization by
414 methoxybenzaldehydes and AN photolysis. Correspondingly, nitroaromatic compounds and N-heterocycles are frequently
415 noted in BBOA (Iinuma et al., 2010; Kitanovski et al., 2012; Kourtchev et al., 2016) and have been proposed to be potential
416 contributors to BrC light absorption (Laskin et al., 2015). Relative to GUA+DMB+AN and GUA+VL+AN, only 19% of the
417 N-containing products in GUA+AN were potential BrC chromophores (Fig. S8e,f), and these did not include CHN species.
418 These indicate that the N-containing products formed in the presence of both photosensitizers and AN may be more
419 significant contributors to the light absorption of phenolic aqSOA than those formed in AN only.

420 **4 Conclusions and atmospheric implications**

421 The photosensitized oxidation of guaiacol (GUA) by triplet excited states of 3,4-dimethoxybenzaldehyde (³DMB*) and
422 vanillin (³VL*) (separately) in the absence and presence of ammonium nitrate (AN) were compared under identical

423 conditions (simulated sunlight and concentration) relevant to atmospheric cloud and fog waters. Compared to GUA+VL,
424 faster GUA oxidation and stronger light absorption by the products were observed in GUA+DMB. Moreover, VL was
425 consumed faster relative to DMB, limiting the extent of GUA oxidation in GUA+VL. These differences are rooted in DMB
426 having a better photosensitizing ability than VL and the -OH group of VL, making it more susceptible to oxidation and more
427 reactive towards electrophilic aromatic substitution. Both GUA+DMB and GUA+VL generated aqSOA (including potential
428 BrC chromophores) composed of oligomers, functionalized monomers, oxygenated ring-opening products, and N-containing
429 products in the presence of AN. The major aqSOA formation processes for GUA+DMB and GUA+VL were oligomerization
430 and functionalization, but functionalization appeared to be more significant in GUA+VL due to VL transformation products.
431 The photochemical evolution of aqSOA from GUA+DMB has been reported by Yu et al. (2016). Similar experiments for
432 aqSOA from GUA+VL should be conducted in the future to better understand photosensitized reactions involving phenolic
433 carbonyl photosensitizers.

434 AN did not significantly affect the decay kinetics due to the predominant effect of ³DMB* and ³VL* chemistry
435 compared to nitrate, but it promoted the formation of N-containing products; these are composed of N-heterocycles (e.g.,
436 imidazoles) and oligomers and nitrated species. The observation of N-heterocycles agrees with our previous findings that
437 ammonium participates in photosensitized oxidation of phenolic compounds in the presence of AN (Mabato et al., 2022).
438 These results also suggest that photosensitized oxidation of phenolic compounds in the presence of AN might be an
439 important source of N-heterocycles and nitrated products. Identifying the sources of N-heterocycles and nitrated compounds
440 is important due to their environmental and health impacts (Laskin et al., 2009). Moreover, photosensitized reactions by non-
441 phenolic and phenolic methoxybenzaldehydes may be differently influenced by AN photolysis. For instance, the more
442 extensive fragmentation in GUA+DMB than in GUA+VL possibly resulted in more N-containing products in
443 GUA+DMB+AN. Furthermore, the increased oligomers in GUA+VL+AN may be due to VL-derived phenoxy radicals
444 induced by [•]OH or [•]NO₂ from nitrate photolysis. In addition, more nitrated compounds observed in GUA+DMB+AN and
445 GUA+VL+AN than in GUA+AN imply that photosensitized reactions may promote nitrate-mediated photolytic reactions.
446 On a related note, the significance of photosensitization by BrC (via formation of solvated electrons; Y. Wang et al., 2021)
447 and marine dissolved organic matter (via O₂^{•-} formation; Garcia et al., 2021) in enhanced nitrite production from nitrate
448 photolysis have been reported. A recent study from our group has shown that glyoxal photo-oxidation mediated by both
449 nitrate photolysis and photosensitization can significantly enhance the atmospheric sink of glyoxal (Zhang et al., 2022).
450 Further studies are needed to improve our understanding of the interplay between photosensitized reactions and nitrate
451 photolysis.

452 This study demonstrates that the structural features of photosensitizers affect aqSOA formation via non-carbonyl
453 phenol oxidation. The VL results are broadly relevant to other phenolic carbonyls, but the effects of different functional
454 groups should still be considered. For instance, the aldehyde/ketone pair of syringaldehyde and acetosyringone, both
455 phenolic carbonyls, have been reported to have equal reactivity towards direct photosensitized oxidation. This is due to the
456 greater light absorption by the aldehyde form but higher quantum efficiency for loss for the ketone form (Smith et al. 2016).

457 However, more aqSOA was observed from syringaldehyde than acetosyringone (in either AN or ammonium sulfate; Huang
458 et al., 2018). Our findings also imply that while the contributions of photosensitization by ³VL* (and other phenolic
459 carbonyls) to aqSOA formation would be relatively less compared to that of ³DMB* (and other non-phenolic carbonyls),
460 these are not negligible. As both non-phenolic and phenolic carbonyls such as the methoxybenzaldehydes examined in this
461 work are emitted in large amounts from biomass burning, future experiments should probe the aqSOA contribution of a
462 wider variety of photosensitizers. Moreover, further experiments on photosensitized reactions in authentic particulate matter
463 (PM) samples should be conducted in the future. Multicomponent reactions such as GUA+DMB+AN and GUA+VL+AN
464 should also be explored for a more accurate simulation of ambient conditions. These would be useful in assessing the overall
465 impact of photosensitized reactions and AN photolysis on aqSOA formation in areas impacted by biomass burning and high
466 AN concentrations, and for their better representation in aqSOA models.

467

468 *Data availability.*

469 The data used in this publication are available to the community and can be accessed by request to the corresponding author.

470 *Author contributions.*

471 BRGM designed and conducted the experiments; BRGM and CKC wrote the paper. All co-authors contributed to the
472 discussion of the manuscript.

473 *Competing interests.*

474 The authors declare that they have no conflict of interest.

475 *Acknowledgments.*

476 C.K.C. gratefully acknowledges support from the National Natural Science Foundation of China (42075100, 41875142, and
477 42275104) and Hong Kong Research Grants Council (11304121). Y.J.L. acknowledges funding support from the Science
478 and Technology Development Fund, Macau SAR (File No. 0019/2020/A1), and a multiyear research grant (No.
479 MYRG2018-00006-FST) from the University of Macau. The authors also thank the University Research Facility in
480 Chemical and Environmental Analysis (UCEA) at The Hong Kong Polytechnic University for the use of its UHPLC-HESI-
481 Orbitrap Mass Spectrometer and Dr Sirius Tse and Dr Chi Hang Chow for assistance with sample analyses.

482 **References**

483 Anastasio, C., Faust, B. C., and Rao, C. J.: Aromatic carbonyl compounds as aqueous-phase photochemical sources of
484 hydrogen peroxide in acidic sulfate aerosols, fogs, and clouds. 1. Non-phenolic methoxybenzaldehydes and
485 methoxyacetophenones with reductants (phenols), *Environ. Sci. Technol.*, 31, 218–232, <https://doi.org/10.1021/es960359g>,
486 1997.

487

488 Bateman, A. P., Laskin, J., Laskin, A., and Nizkorodov, S. A.: Applications of high-resolution electrospray ionization mass
489 spectrometry to measurements of average oxygen to carbon ratios in secondary organic aerosols, *Environ. Sci. Technol.*, 46,
490 8315–832, <https://doi.org/10.1021/es3017254>, 2012.

491 Bianco, A., Passananti, M., Brigante, M., and Mailhot, G.: Photochemistry of the cloud aqueous phase: a review, *Molecules*,
492 25, 423, <https://doi.org/10.3390/molecules25020423>, 2020.
493

494 Calvert, J. G. and Madronich, S.: Theoretical study of the initial products of the atmospheric oxidation of hydrocarbons, *J.*
495 *Geophys. Res.*, 92, 2211–2220, <https://doi.org/10.1029/JD092iD02p02211>, 1987.
496

497 Chen, Y., Li, N., Li, X., Tao, Y., Luo, S., Zhao, Z., Ma, S., Huang, H., Chen, Y., Ye, Z., and Ge, X.: Secondary organic
498 aerosol formation from ³C*-initiated oxidation of 4-ethylguaiaicol in atmospheric aqueous-phase, *Sci. Total Environ.*, 723,
499 137953, <https://doi.org/10.1016/j.scitotenv.2020.137953>, 2020.
500

501 Chen, Z. and Anastasio, C.: Concentrations of a triplet excited state are enhanced in illuminated ice, *Environ. Sci.: Processes*
502 *Impacts*, 19, 12–21, <https://doi.org/10.1039/C6EM00534A>, 2017.
503

504 Collett, J. L. Jr., Hoag, K. J., Sherman, D. E., Bator, A., and Richards, L. W.: Spatial and temporal variations in San Joaquin
505 Valley fog chemistry, *Atmos. Environ.*, 33, 129–140, [https://doi.org/10.1016/S1352-2310\(98\)00136-8](https://doi.org/10.1016/S1352-2310(98)00136-8), 1998.
506

507 De Haan, D. O., Tolbert, M. A., and Jimenez, J. L.: Atmospheric condensed-phase reactions of glyoxal with methylamine,
508 *Geophys. Res. Lett.*, 36, No. L11819, <https://doi.org/10.1029/2009GL037441>, 2009.
509

510 De Haan, D. O., Hawkins, L. N., Kononenko, J. A., Turley, J. J., Corrigan, A. L., Tolbert, M. A., and Jimenez, J. L.:
511 Formation of nitrogen-containing oligomers by methylglyoxal and amines in simulated evaporating cloud droplets, *Environ.*
512 *Sci. Technol.*, 45, 984–991, <https://doi.org/10.1021/es102933x>, 2011.
513

514 De Haan, D. O., Pajunoja, A., Hawkins, L. N., Welsh, H. G., Jimenez, N. G., De Loera, A., Zauscher, M., Andretta, A. D.,
515 Joyce, B. W., De Haan, A. C., Riva, M., Cui, T., Surratt, J. D., Cazaunau, M., Formenti, P., Gratien, A., Pangui, E., and
516 Doussin, J-F.: Methylamine's effects on methylglyoxal-containing aerosol: chemical, physical, and optical changes, *ACS*
517 *Earth Space Chem.*, 3, 1706–1716, <https://doi.org/10.1021/acsearthspacechem.9b00103>, 2019.
518

519 Du, Y., Fu, Q. S., Li, Y., and Su, Y.: Photodecomposition of 4-chlorophenol by reactive oxygen species in UV/air system, *J.*
520 *Hazard. Mater.*, 186, 491–496, <https://doi.org/10.1016/j.jhazmat.2010.11.023>, 2011.
521

522 Edye, L. A. and Richards, G. N.: Analysis of condensates from wood smoke. components derived from polysaccharides and
523 lignins, *Environ. Sci. Technol.*, 25, 1133–1137, <https://doi.org/10.1021/es00018a018>, 1991.
524

525 Felber, T., Schaefer, T., He, L., and Herrmann, H.: Aromatic carbonyl and nitro compounds as photosensitizers and their
526 photophysical properties in the tropospheric aqueous phase, *J. Phys. Chem. A*, 125, 5078–5095,
527 <https://doi.org/10.1021/acs.jpca.1c03503>, 2021.
528

529 Fleming, L. T., Lin, P., Laskin, A., Laskin, J., Weltman, R., Edwards, R. D., Arora, N. K., Yadav, A., Meinardi, S., Blake, D.
530 R., Pillarisetti, A., Smith, K. R., and Nizkorodov, S. A.: Molecular composition of particulate matter emissions from dung
531 and brushwood burning household cookstoves in Haryana, India, *Atmos. Chem. Phys.*, 18, 2461–2480,
532 <https://doi.org/10.5194/acp-18-2461-2018>, 2018.
533

534 Galloway, M. M., Chhabra, P. S., Chan, A. W. H., Surratt, J. D., Flagan, R. C., Seinfeld, J. H., and Keutsch, F. N.: Glyoxal
535 uptake on ammonium sulphate seed aerosol: reaction products and reversibility of uptake under dark and irradiated
536 conditions, *Atmos. Chem. Phys.*, 9, 3331–3345, <https://doi.org/10.5194/acp-9-3331-2009>, 2009.
537

538 Garcia, S. L. M., Pandit, S., Navea, J. G., and Grassian, V. H.: Nitrous acid (HONO) formation from the irradiation of
539 aqueous nitrate solutions in the presence of marine chromophoric dissolved organic matter: comparison to other organic
540 photosensitizers, *ACS Earth Space Chem.*, 5, 3056–3064, <https://doi.org/10.1021/acsearthspacechem.1c00292>, 2021.

541 Gen, M., Huang, D. D., and Chan, C. K.: Reactive uptake of glyoxal by ammonium-containing salt particles as a function of
542 relative humidity, *Environ. Sci. Technol.*, 52, 6903–6911, <https://doi.org/10.1021/acs.est.8b00606>, 2018.

543

544 Gen, M., Zhang, R., Huang, D. D., Li, Y. J., and Chan, C. K.: Heterogeneous SO₂ oxidation in sulfate formation by
545 photolysis of particulate nitrate, *Environ. Sci. Technol. Lett.*, 6, 86–91, <https://doi.org/10.1021/acs.estlett.8b00681>, 2019a.

546

547 Gen, M., Zhang, R., Huang, D. D., Li, Y. J., and Chan, C. K.: Heterogeneous oxidation of SO₂ in sulfate production during
548 nitrate photolysis at 300 nm: effect of pH, relative humidity, irradiation intensity, and the presence of organic compounds,
549 *Environ. Sci. Technol.*, 53, 8757–8766, <https://doi.org/10.1021/acs.est.9b01623>, 2019b.

550

551 Gen, M., Liang, Z., Zhang, R., Mabato, B. R. G., and Chan, C. K.: Particulate nitrate photolysis in the atmosphere, *Environ.*
552 *Sci.: Atmos.*, 2, 111–127, <https://doi.org/10.1039/d1ea00087j>, 2022.

553

554 George, C., Brüggemann, M., Hayeck, N., Tinel, L., and Donaldson, J.: Interfacial photochemistry: physical chemistry of
555 gas-liquid interfaces, in: *Developments in Physical & Theoretical Chemistry*, edited by: Faust, J. A. and House, J. E.,
556 Elsevier, 435–457, <https://doi.org/10.1016/B978-0-12-813641-6.00014-5>, 2018.

557

558 Giulianelli, L., Gilardoni, S., Tarozzi, L., Rinaldi, M., Decesari, S., Carbone, C., Facchini, M. C., and Fuzzi, S.: Fog
559 occurrence and chemical composition in the Po valley over the last twenty years, *Atmos. Environ.*, 98, 394–401,
560 <https://doi.org/10.1016/j.atmosenv.2014.08.080>, 2014.

561

562 Grace, D. N., Sharp, J. R., Holappa, R. E., Lugos, E. N., Sebold, M. B., Griffith, D. R., Hendrickson, H. P., and Galloway,
563 M. M.: Heterocyclic product formation in aqueous brown carbon systems, *ACS Earth Space Chem.*, 3, 2472–2481,
564 <https://doi.org/10.1021/acsearthspacechem.9b00235>, 2019.

565

566 Hawthorne, S. B., Miller, D. J., Langenfeld, J. J., and Krieger, M. S.: PM-10 High-volume collection and quantitation of
567 semi- and nonvolatile phenols, methoxylated phenols, alkanes, and polycyclic aromatic hydrocarbons from winter urban air
568 and their relationship to wood smoke emissions, *Environ. Sci. Technol.*, 26, 2251–2262,
569 <https://doi.org/10.1021/es00035a026>, 1992.

570

571 Hems, R. F., Schnitzler, E. G., Bastawrous, M., Soong, R., Simpson, A. J., and Abbatt, J. P. D.: Aqueous photoreactions of
572 wood smoke brown carbon, *ACS Earth Space Chem.*, 4, 1149–1160, <https://doi.org/10.1021/acsearthspacechem.0c0011>,
573 2020.

574

575 Hoshino, M., Akimoto, H., and Okuda, M.: Photochemical oxidation of benzene, toluene, and ethylbenzene initiated by OH
576 radicals in the gas phase, *Bull. Chem. Soc. Jpn.*, 51, 718–724, <https://doi.org/10.1246/bcsj.51.718>, 1978.

577

578 Huang, D. D., Zhang, Q., Cheung, H. H. Y., Yu, L., Zhou, S., Anastasio, C., Smith, J. D., and Chan, C. K.: Formation and
579 evolution of aqSOA from aqueous-phase reactions of phenolic carbonyls: comparison between ammonium sulfate and
580 ammonium nitrate solutions, *Environ. Sci. Technol.*, 52, 9215–9224, <https://doi.org/10.1021/acs.est.8b03441>, 2018.

581

582 Iinuma, Y., Böge, O., Gräfe, R., and Herrmann, H.: Methyl-nitrocatechols: atmospheric tracer compounds for biomass
583 burning secondary organic aerosols, *Environ. Sci. Technol.*, 44, 8453–8459, <https://doi.org/10.1021/es102938a>, 2010.

584

585 Jiang, W., Misovich, M. V., Hettiyadura, A. P. S., Laskin, A., McFall, A. S., Anastasio, C., and Zhang, Q.: Photosensitized
586 reactions of a phenolic carbonyl from wood combustion in the aqueous phase—chemical evolution and light absorption
587 properties of aqSOA, *Environ. Sci. Technol.*, 55, 5199–5211, <https://doi.org/10.1021/acs.est.0c07581>, 2021.

588

589 Kampf, C. J., Jakob, R., and Hoffmann, T.: Identification and characterization of aging products in the glyoxal/ammonium
590 sulfate system – implications for light-absorbing material in atmospheric aerosols, *Atmos. Chem. Phys.*, 12, 6323–6333,
591 <https://doi.org/10.5194/acp-12-6323-2012>, 2012.

592

593 Kebarle, P. A.: A brief overview of the mechanisms involved in electrospray mass spectrometry, *J. Mass Spectrom.*, 35,
594 804–817, <https://doi.org/10.1002/9783527628728.ch1>, 2000.

595

596 Kitanovski, Z., Grgić, I., Vermeulen, R., Claeys, M., and Maenhaut, W.: Liquid chromatography tandem mass spectrometry
597 method for characterization of monoaromatic nitro-compounds in atmospheric particulate matter, *J. Chromatogr. A*, 1268,
598 35–43, <https://doi.org/10.1016/j.chroma.2012.10.021>, 2012.

599

600 Klodt, A.L., Romonosky, D.E., Lin, P., Laskin, J., Laskin, A., and Nizkorodov, S.A.: Aqueous photochemistry of secondary
601 organic aerosol of α -pinene and α -humulene in the presence of hydrogen peroxide or inorganic salts, *ACS Earth Space*
602 *Chem.*, 3, 12, 2736–2746, <https://doi.org/10.1021/acsearthspacechem.9b00222>, 2019.

603

604 Kobayashi, S. and Higashimura, H.: Oxidative polymerization of phenols revisited, *Prog. Polym. Sci.*, 28, 1015–1048,
605 [https://doi.org/10.1016/S0079-6700\(03\)00014-5](https://doi.org/10.1016/S0079-6700(03)00014-5), 2003.

606

607 Kourtshev, I., Fuller, S. J., Giorio, C., Healy, R. M., Wilson, E., O’Connor, I., Wenger, J. C., McLeod, M., Aalto, J.,
608 Ruuskanen, T. M., Maenhaut, W., Jones, R., Venables, D. S., Sodeau, J. R., Kulmala, M., and Kalberer, M.: Molecular
609 composition of biogenic secondary organic aerosols using ultrahigh-resolution mass spectrometry: comparing laboratory and
610 field studies, *Atmos. Chem. Phys.*, 14, 2155–2167, <https://doi.org/10.5194/acp-14-2155-2014>, 2014.

611

612 Kourtshev, I., Godoi, R. H. M., Connors, S., Levine, J. G., Archibald, A. T., Godoi, A. F. L., Paralovo, S. L., Barbosa, C. G.
613 G., Souza, R. A. F., Manzi, A. O., Seco, R., Sjostedt, S., Park, J., Guenther, A., Kim, S., Smith, J., Martin, S. T., and
614 Kalberer, M.: Molecular composition of organic aerosols in central Amazonia: an ultra-high-resolution mass spectrometry
615 study, *Atmos. Chem. Phys.*, 16, 11899–11913, <https://doi.org/10.5194/acp-16-11899-2016>, 2016.

616

617 Kroll, J. H., Donahue, N. M., Jimenez, J. L., Kessler, S. H., Canagaratna, M. R., Wilson, K. R., Altieri, K. E., Mazzoleni, L.
618 R., Wozniak, A. S., Bluhm, H., Mysak, E. R., Smith, J. D., Kolb, C. E., and Worsnop, D. R.: Carbon oxidation state as a
619 metric for describing the chemistry of atmospheric organic aerosol, *Nat. Chem.*, 3, 133–139,
620 <https://doi.org/10.1038/nchem.948>, 2011.

621

622 Krueve, A., Kaupmees, K., Liigand, J., and Leito, I.: Negative electrospray ionization via deprotonation: predicting the
623 ionization efficiency, *Anal. Chem.*, 86, 4822–4830, <https://doi.org/10.1021/ac404066v>, 2014.

624

625 Laskin, A., Smith, J. S., and Laskin, J.: Molecular characterization of nitrogen-containing organic compounds in biomass
626 burning aerosols using high-resolution mass spectrometry, *Environ. Sci. Technol.*, 43, 3764–3771,
627 <https://doi.org/10.1021/es803456n>, 2009.

628

629 Laskin, A., Laskin, J., and Nizkorodov, S. A.: Chemistry of atmospheric brown carbon, *Chem. Rev.*, 115, 4335–4382,
630 <https://doi.org/10.1021/cr5006167>, 2015.

631

632 Laskin, J., Laskin, A., Nizkorodov, S. A., Roach, P., Eckert, P., Gilles, M. K., Wang, B., Lee, H. J., and Hu, Q.: Molecular
633 selectivity of brown carbon chromophores, *Environ. Sci. Technol.*, 48, 12047–12055, <https://doi.org/10.1021/es503432r>,
634 2014.

635

636 Lee, A. K. Y., Zhao, R., Li, R., Liggio, J., Li, S., and Abbatt, J. P. D.: Formation of light absorbing organo-nitrogen species
637 from evaporation of droplets containing glyoxal and ammonium sulfate, *Environ. Sci. Technol.*, 47, 12819–12826,
638 <https://doi.org/10.1021/es402687w>, 2013.

639 Lee, H. J., Aiona, P. K., Laskin, A., Laskin, J., and Nizkorodov, S. A.: Effect of solar radiation on the optical properties and
640 molecular composition of laboratory proxies of atmospheric brown carbon, *Environ. Sci. Technol.*, 48, 10217–10226,
641 <https://doi.org/10.1021/es502515r>, 2014.

642

643 Leifer, A.: *The Kinetics of environmental aquatic photochemistry: Theory and practice*, American Chemical Society,
644 Washington, DC, 1988.

645

646 Leito, I., Herodes, K., Huopola, M., Virro, K., Künnapas, A., Krueve, A., and Tanner, R.: Towards the electrospray
647 ionization mass spectrometry ionization efficiency scale of organic compounds, *Rapid Commun. Mass Sp.*, 22, 379–384,
648 <https://doi.org/10.1002/rcm.3371>, 2008.

649

650 Li, P., Li, X., Yang, C., Wang, X., Chen, J., and Collett, J. L. Jr.: Fog water chemistry in Shanghai, *Atmos. Environ.*, 45,
651 4034–4041, <https://doi.org/10.1016/j.atmosenv.2011.04.036>, 2011.

652

653 Li, Y. J., Huang, D. D., Cheung, H. Y., Lee, A. K. Y., and Chan, C. K.: Aqueous-phase photochemical oxidation and direct
654 photolysis of vanillin - a model compound of methoxy phenols from biomass burning, *Atmos. Chem. Phys.*, 14, 2871–2885,
655 <https://doi.org/10.5194/acp-14-2871-2014>, 2014.

656

657 Liang, Z., Zhang, R., Gen, M., Chu, Y., and Chan, C. K.: Nitrate photolysis in mixed sucrose–nitrate–sulfate particles at
658 different relative humidities, *J. Phys. Chem. A*, 125, 3739–3747, <https://doi.org/10.1021/acs.jpca.1c00669>, 2021.

659

660 Lin, P., Yu, J. Z., Engling, G., and Kalberer, M.: Organosulfates in humic-like substance fraction isolated from aerosols at
661 seven locations in East Asia: a study by ultra-high-resolution mass spectrometry, *Environ. Sci. Technol.*, 46, 13118–13127,
662 <https://doi.org/10.1021/es303570v>, 2012.

663

664 Lin, P., Fleming, L. T., Nizkorodov, S. A., Laskin, J., and Laskin, A.: Comprehensive molecular characterization of
665 atmospheric brown carbon by high resolution mass spectrometry with electrospray and atmospheric pressure
666 photoionization, *Anal. Chem.*, 90, 12493–12502, <https://doi.org/10.1021/acs.analchem.8b02177>, 2018.

667

668 Lipari, F., Dasch, J. M., and Scruggs, W. F.: Aldehyde emissions from wood-burning fireplaces, *Environ. Sci. Technol.*, 18,
669 326–330, <https://doi.org/10.1021/es00123a007>, 1984.

670

671 Liu, C., Chen, D., and Chen, X.: Atmospheric reactivity of methoxyphenols: a review, *Environ. Sci. Technol.*, 56, 2897–
672 2916, <https://doi.org/10.1021/acs.est.1c06535>, 2022.

673

674 Lobodin, V. V., Marshall, A. G., and Hsu, C. S.: Compositional space boundaries for organic compounds, *Anal. Chem.*, 84,
675 3410–3416, <https://doi.org/10.1021/ac300244f>, 2012.

676

677 Mabato, B. R. G., Gen, M., Chu, Y., and Chan, C. K.: Reactive uptake of glyoxal by methylammonium-containing salts as a
678 function of relative humidity, *ACS Earth Space Chem.*, 3, 150–157, <https://doi.org/10.1021/acsearthspacechem.8b00154>,
679 2019.

680

681 Mabato, B. R. G., Lyu, Y., Ji, Y., Li, Y. J., Huang, D. D., Li, X., Nah, T., Lam, C. H., and Chan, C. K.: Aqueous secondary
682 organic aerosol formation from the direct photosensitized oxidation of vanillin in the absence and presence of ammonium
683 nitrate, *Atmos. Chem. Phys.*, 22, 273–293, <https://doi.org/10.5194/acp-22-273-2022>, 2022.

684

685 Mazzoleni, L. R., Saranjampour, P., Dalbec, M. M., Samburova, V., Hallar, A. G., Zielinska, B., Lowenthal, D. H., and
686 Kohl, S.: Identification of water-soluble organic carbon in non-urban aerosols using ultrahigh-resolution FT-ICR mass
687 spectrometry: organic anions, *Environ. Chem.*, 9, 285–297, <https://doi.org/10.1071/EN11167>, 2012.

688 Minero, C., Bono, F., Rubertelli, F., Pavino, D., Maurino, V., Pelizzetti, E., and Vione, D.: On the effect of pH in aromatic
689 photonitration upon nitrate photolysis, *Chemosphere*, 66, 650–656, <https://doi.org/10.1016/j.chemosphere.2006.07.082>, 2007.
690

691 Misovich, M. V., Hettiyadura, A. P. S., Jiang, W., Zhang, Q., and Laskin, A.: Molecular-level study of the photo-oxidation
692 of aqueous-phase guaiacyl acetone in the presence of $^3\text{C}^*$: formation of brown carbon products, *ACS Earth Space Chem.*, 5,
693 1983–1996, <https://doi.org/10.1021/acsearthspacechem.1c00103>, 2021.
694

695 Munger, J. W., Jacob, D. J., Waldman, J. M., and Hoffmann, M. R.: Fogwater chemistry in an urban atmosphere, *J.*
696 *Geophys. Res. [Oceans]*, 88, 5109–5121, <https://doi.org/10.1029/JC088iC09p05109>, 1983.
697

698 Ning, C., Gao, Y., Zhang, H., Yu, H., Wang, L., Geng, N., Cao, R., and Chen, J.: Molecular characterization of dissolved
699 organic matters in winter atmospheric fine particulate matters (PM_{2.5}) from a coastal city of northeast China, *Sci. Total*
700 *Environ.*, 689, 312–321, <https://doi.org/10.1016/j.scitotenv.2019.06.418>, 2019.
701

702 Nolte, C. G., Schauer, J. J., Cass, G. R., and Simoneit, B. R. T.: Highly polar organic compounds present in wood smoke and
703 in the ambient atmosphere, *Environ. Sci. Technol.*, 35, 1912–1919, <https://doi.org/10.1021/es001420r>, 2001.
704

705 Nozière, B., Dziedzic, P., and Córdova, A.: Products and kinetics of the liquid-phase reaction of glyoxal catalyzed by
706 ammonium ions (NH_4^+), *J. Phys. Chem. A*, 113, 231–237, <https://doi.org/10.1021/jp8078293>, 2009.
707

708 Nozière, B., Dziedzic, P., and Córdova, A.: Inorganic ammonium salts and carbonate salts are efficient catalysts for aldol
709 condensation in atmospheric aerosols, *Phys. Chem. Chem. Phys.*, 12, 3864–3872, <https://doi.org/10.1039/B924443C>, 2010.
710

711 Nozière, B., Fache, F., Maxut, A., Fenet, B., Baudouin, A., Fine, L., and Ferronato, C.: The hydrolysis of epoxides catalyzed
712 by inorganic ammonium salts in water: kinetic evidence for hydrogen bond catalysis, *Phys. Chem. Chem. Phys.*, 20,
713 1583–1590, <https://doi.org/10.1039/C7CP06790A>, 2018.
714

715 Pang, H., Zhang, Q., Lu, X., Li, K., Chen, H., Chen, J., Yang, X., Ma, Y., Ma, J., and Huang, C.: Nitrite-mediated
716 photooxidation of vanillin in the atmospheric aqueous phase, *Environ. Sci. Technol.*, 53, 14253–14263,
717 <https://doi.org/10.1021/acs.est.9b03649>, 2019.
718

719 Perry, R. H., Cooks, R. G., and Noll, R. J.: Orbitrap mass spectrometry: instrumentation, ion motion and applications, *Mass*
720 *Spectrom. Rev.*, 27, 661–699, <https://doi.org/10.1002/mas.20186>, 2008.
721

722 Powelson, M. H., Espelien, B. M., Hawkins, L. N., Galloway, M. M., and De Haan, D. O.: Brown carbon formation by
723 aqueous-phase carbonyl compound reactions with amines and ammonium sulfate, *Environ. Sci. Technol.*, 48, 985–993,
724 <https://doi.org/10.1021/es4038325>, 2014.
725

726 Pye, H. O. T., Nenes, A., Alexander, B., Ault, A. P., Barth, M. C., Clegg, S. L., Collett, J. L. Jr., Fahey, K. M., Hennigan, C.
727 J., Herrmann, H., Kanakidou, M., Kelly, J. T., Ku, I., McNeill, V. F., Riemer, N., Schaefer, T., Shi, G., Tilgner, A., Walker,
728 J. T., Wang, T., Weber, R., Xing, J., Zaveri, R. A., and Zuend, A.: The acidity of atmospheric particles and clouds, *Atmos.*
729 *Chem. Phys.*, 20, 4809–4888, <https://doi.org/10.5194/acp-20-4809-2020>, 2020.
730

731 Raja, S., Raghunathan, R., Yu, X., Lee, T., Chen, J., Kommalapati, R. R., Murugesan, K., Shen, X., Qingzhong, Y., Valsaraj,
732 K. T., and Collett, J. L. Jr.: Fog chemistry in the Texas-Louisiana Gulf Coast corridor, *Atmos. Environ.*, 42, 2048–2061,
733 <https://doi.org/10.1016/j.atmosenv.2007.12.004>, 2008.
734

735 Rogge, W. F., Hildemann, L. M., Mazurek, M. A., and Cass, G. R.: Sources of fine organic aerosol. 9. Pine, oak, and
736 synthetic log combustion in residential fireplaces, *Environ. Sci. Technol.*, 32, 13–22, <https://doi.org/10.1021/es960930b>,
737 1998.

738 Romonosky, D. E., Li, Y., Shiraiwa, M., Laskin, A., Laskin, J., and Nizkorodov, S. A.: Aqueous photochemistry of
739 secondary organic aerosol of α -Pinene and α -Humulene oxidized with ozone, hydroxyl radical, and nitrate radical, *J. Phys.*
740 *Chem. A*, 121, 1298–1309, <https://doi.org/10.1021/acs.jpca.6b10900>, 2017.

741

742 Sagebiel, J. C., Seiber, J. N., and Woodrow, J. E.: Comparison of headspace and gas-stripping methods for determining the
743 Henry's law constant (H) for organic compounds of low to intermediate H, *Chemosphere*, 25, 1763–1768,
744 [https://doi.org/10.1016/0045-6535\(92\)90017-L](https://doi.org/10.1016/0045-6535(92)90017-L), 1992.

745

746 Schauer, J. J., Kleeman, M. J., Cass, G. R., and Simoneit, B. R. T.: Measurement of emissions from air pollution sources. 3.
747 C₁-C₂₉ organic compounds from fireplace combustion of wood, *Environ. Sci. Technol.*, 35, 1716–1728,
748 <https://doi.org/10.1021/es001331e>, 2001.

749

750 Schmidt, A-C., Herzsuh, R., Matysik, F-M., and Engewald, W.: Investigation of the ionisation and fragmentation
751 behaviour of different nitroaromatic compounds occurring as polar metabolites of explosives using electrospray ionisation
752 tandem mass spectrometry, *Rapid Commun. Mass Sp.*, 20, 2293–2302, <https://doi.org/10.1002/rcm.2591>, 2006.

753

754 Shapiro, E. L., Szprengiel, J., Sareen, N., Jen, C. N., Giordano, M. R., and McNeill, V. F.: Light-absorbing secondary
755 organic material formed by glyoxal in aqueous aerosol mimics, *Atmos. Chem. Phys.*, 9, 2289–2300,
756 <https://doi.org/10.5194/acp-9-2289-2009>, 2009.

757

758 Siegmann, K. and Sattler, K.: Formation mechanism for polycyclic aromatic hydrocarbons in methane flames, *J. Chem.*
759 *Phys.*, 112, 698–709, <https://doi.org/10.1063/1.480648>, 2000.

760

761 Simoneit, B. R. T.: Biomass burning — a review of organic tracers for smoke from incomplete combustion, *Appl.*
762 *Geochem.*, 17, 129–162, [https://doi.org/10.1016/S0883-2927\(01\)00061-0](https://doi.org/10.1016/S0883-2927(01)00061-0), 2002.

763

764 Simoneit, B. R. T., Rogge, W. F., Mazurek, M. A., Standley, L. J., Hildemann, L. M., and Cass, G. R.: Lignin pyrolysis
765 products, lignans, and resin acids as specific tracers of plant classes in emissions from biomass combustion, *Environ. Sci.*
766 *Technol.*, 27, 2533–2541, <https://doi.org/10.1021/es00048a034>, 1993.

767

768 Simoneit, B. R. T., Schauer, J. J., Nolte, C. G., Oros, D. R., Elias, V. O., Fraser, M. P., Rogge, W. F., and Cass, G. R.:
769 Levoglucosan, a tracer for cellulose in biomass burning and atmospheric particles, *Atmos. Environ.*, 33, 173–182,
770 [https://doi.org/10.1016/S1352-2310\(98\)00145-9](https://doi.org/10.1016/S1352-2310(98)00145-9), 1999.

771

772 Simpson, C. D., Paulsen, M., Dills, R. L., Liu, L.-J. S., and Kalman, D. A.: Determination of methoxyphenols in ambient
773 atmospheric particulate matter: tracers for wood combustion, *Environ. Sci. Technol.*, 39, 631–637,
774 <https://doi.org/10.1021/es0486871>, 2005.

775

776 Slikboer, S., Grandy, L., Blair, S. L., Nizkorodov, S. A., Smith, R. W., and Al-Abadleh, H. A.: Formation of light absorbing
777 soluble secondary organics and insoluble polymeric particles from the dark reaction of catechol and guaiacol with Fe(III),
778 *Environ. Sci. Technol.*, 49, 7793–7801, <https://doi.org/10.1021/acs.est.5b01032>, 2015.

779

780 Smith, D. F., Kleindienst, T. E., and McIver, C. D.: Primary product distributions from the reaction of OH with m-, p-xylene,
781 1,2,4- and 1,3,5-trimethylbenzene, *J. Atmos. Chem.*, 34, 339–364, <https://doi.org/10.1023/A:1006277328628>, 1999.

782

783 Smith, J. D., Sio, V., Yu, L., Zhang, Q., and Anastasio, C.: Secondary organic aerosol production from aqueous reactions of
784 atmospheric phenols with an organic triplet excited state, *Environ. Sci. Technol.*, 48, 1049–1057,
785 <https://doi.org/10.1021/es4045715>, 2014.

786 Smith, J. D., Kinney, H., and Anastasio, C.: Aqueous benzene-diols react with an organic triplet excited state and hydroxyl
787 radical to form secondary organic aerosol, *Phys. Chem. Chem. Phys.*, 17, 10227–10237,
788 <https://doi.org/10.1039/C4CP06095D>, 2015.

789

790 Smith, J. D., Kinney, H., and Anastasio, C.: Phenolic carbonyls undergo rapid aqueous photodegradation to form low-
791 volatility, light-absorbing products, *Atmos. Environ.*, 126, 36–44, <https://doi.org/10.1016/j.atmosenv.2015.11.035>, 2016.

792

793 Song, J., Li, M., Jiang, B., Wei, S., Fan, X., and Peng, P.: Molecular characterization of water-soluble humic like substances
794 in smoke particles emitted from combustion of biomass materials and coal using ultrahigh-resolution electrospray ionization
795 Fourier transform ion cyclotron resonance mass spectrometry, *Environ. Sci. Technol.*, 52, 2575–2585,
796 <https://doi.org/10.1021/acs.est.7b06126>, 2018.

797

798 Sun, Y. L., Zhang, Q., Anastasio, C., and Sun, J.: Insights into secondary organic aerosol formed via aqueous-phase
799 reactions of phenolic compounds based on high resolution mass spectrometry, *Atmos. Chem. Phys.*, 10, 4809–4822,
800 <https://doi.org/10.5194/acp-10-4809-2010>, 2010.

801

802 US EPA: Estimation Programs Interface Suite™ for Microsoft® Windows, v 4.1, United States Environmental Protection
803 Agency, Washington, DC, USA, 2012.

804

805 Wang, K., Huang, R.-J., Brüggemann, M., Zhang, Y., Yang, L., Ni, H., Guo, J., Wang, M., Han, J., Bilde, M., Glasius, M.,
806 and Hoffmann, T.: Urban organic aerosol composition in eastern China differs from north to south: molecular insight from a
807 liquid chromatography–mass spectrometry (Orbitrap) study, *Atmos. Chem. Phys.*, 21, 9089–9104,
808 <https://doi.org/10.5194/acp-21-9089-2021>, 2021.

809

810 Wang, X., Hayeck, N., Brüggemann, M., Yao, L., Chen, H., Zhang, C., Emmelin, C., Chen, J., George, C., and Wang, L.:
811 Chemical characterization of organic aerosols in Shanghai: A study by ultrahigh-performance liquid chromatography
812 coupled with orbitrap mass spectrometry, *J. Geophys. Res. Atmos.*, 122, 11703–11722,
813 <https://doi.org/10.1002/2017JD026930>, 2017.

814

815 Wang, Y., Huang, D. D., Huang, W., Liu, B., Chen, Q., Huang, R., Gen, M., Mabato, B. R. G., Chan, C. K., Li, X., Hao, T.,
816 Tan, Y., Hoi, K. I., Mok, K. M., and Li, Y. J.: Enhanced nitrite production from the aqueous photolysis of nitrate in the
817 presence of vanillic acid and implications for the roles of light-absorbing organics, *Environ. Sci. Technol.*, 55, 15694–15704,
818 <https://doi.org/10.1021/acs.est.1c04642>, 2021.

819

820 Wang, Y., Huang, W., Tian, L., Wang, Y., Li, F., Huang, D. D., Zhang, R., Mabato, B. R. G., Huang, R., Chen, Q., Ge, X.,
821 Du, L., Ma, Y. G., Gen, M., Hoi, K. I., Mok, K. M., Yu, J. Z., Chan, C. K., Li, X., and Li, Y. J.: Decay kinetics and
822 absorption changes of methoxyphenols and nitrophenols during nitrate-mediated aqueous photochemical oxidation at 254
823 and 313 nm, *ACS Earth Space Chem.*, 6, 1115–1125, <https://doi.org/10.1021/acsearthspacechem.2c00021>, 2022.

824

825 Yang, J., Au, W. C., Law, H., Leung, C. H., Lam, C. H., and Nah, T.: pH affects the aqueous-phase nitrate-mediated
826 photooxidation of phenolic compounds: implications for brown carbon formation and evolution, *Environ. Sci.: Processes
827 Impacts*, <https://doi.org/10.1039/D2EM00004K>, 2022.

828

829 Yasmeen, F., Vermeylen, R., Szmigielski, R., Iinuma, Y., Böge, O., Herrmann, H., Maenhaut, W., and Claeys, M.:
830 Terpenylic acid and related compounds: precursors for dimers in secondary organic aerosol from the ozonolysis of α and β -
831 pinene, *Atmos. Chem. Phys.*, 10, 9383–9392, <https://doi.org/10.5194/acp-10-9383-2010>, 2010.

832

833 Yaws, C. L.: Handbook of vapor pressure, volume 3: Organic compounds C8 to C28, Gulf Professional Publishing, 1994.

834

835 Ye, Z., Qu, Z., Ma, S., Luo, S., Chen, Y., Chen, H., Chen, Y., Zhao, Z., Chen, M., and Ge, X.: A comprehensive
836 investigation of aqueous-phase photochemical oxidation of 4-ethylphenol, *Sci. Total Environ.*, 685, 976–985,
837 <https://doi.org/10.1016/j.scitotenv.2019.06.276>, 2019.

838

839 Yu, G., Bayer, A. R., Galloway, M. M., Korshavn, K. J., Fry, C. G., and Keutsch, F. N.: Glyoxal in aqueous ammonium
840 sulfate solutions: products, kinetics and hydration effects, *Environ. Sci. Technol.*, 45, 6336–6342,
841 <https://doi.org/10.1021/es200989n>, 2011.

842

843 Yu, L., Smith, J., Laskin, A., Anastasio, C., Laskin, J., and Zhang, Q.: Chemical characterization of SOA formed from
844 aqueous-phase reactions of phenols with the triplet excited state of carbonyl and hydroxyl radical, *Atmos. Chem. Phys.*, 14,
845 13801–13816, <https://doi.org/10.5194/acp-14-13801-2014>, 2014.

846

847 Yu, L., Smith, J., Laskin, A., George, K. M., Anastasio, C., Laskin, J., Dillner, A. M., and Zhang, Q.: Molecular
848 transformations of phenolic SOA during photochemical aging in the aqueous phase: competition among oligomerization,
849 functionalization, and fragmentation, *Atmos. Chem. Phys.*, 16, 4511–4527, <https://doi.org/10.5194/acp-16-4511-2016>.

850

851 Zhang, Q. and Anastasio, C.: Conversion of fogwater and aerosol organic nitrogen to ammonium, nitrate, and NO_x during
852 exposure to simulated sunlight and ozone, *Environ. Sci. Technol.*, 37, 3522–3530, <https://doi.org/10.1021/es034114x>, 2003.

853

854 Zhang, R., Gen, M., Huang, D. D., Li, Y. J., and Chan, C. K.: Enhanced sulfate production by nitrate photolysis in the
855 presence of halide ions in atmospheric particles, *Environ. Sci. Technol.*, 54, 3831–3839,
856 <https://doi.org/10.1021/acs.est.9b06445>, 2020.

857

858 Zhang, R., Gen, M., Fu, T.-M., and Chan, C. K.: Production of formate via oxidation of glyoxal promoted by particulate
859 nitrate photolysis, *Environ. Sci. Technol.*, 55, 5711–5720, <https://doi.org/10.1021/acs.est.0c0819>, 2021.

860

861 Zhang, R., Gen, M., Liang, Z., Li, Y. J., and Chan, C. K.: Photochemical reactions of glyoxal during particulate ammonium
862 nitrate photolysis: Brown carbon formation, enhanced glyoxal decay, and organic phase formation, *Environ. Sci. Technol.*,
863 56, 1605–1614, <https://doi.org/10.1021/acs.est.1c07211>, 2022.

864

865 Zielinski, T., Bolzacchini, E., Cataldi, M., Ferrero, L., Graßl, S., Hansen, G., Mateos, D., Mazzola, M., Neuber, R., Pakszys,
866 P., Posyniak, M., Ritter, C., Severi, M., Sobolewski, P., Traversi, R., and Velasco-Merino, C.: Study of chemical and optical
867 properties of biomass burning aerosols during long-range transport events toward the Arctic in summer 2017, *Atmosphere*,
868 11, 84, <https://doi.org/10.3390/atmos11010084>, 2020.

869

870

871

872

873

874

875

876

877

878

879

880

881 **Table 1.** Reaction conditions, initial GUA (and DMB or VL) decay rate constants, normalized abundance of products,
 882 average elemental ratios, and average carbon oxidation state ($\langle OS_C \rangle$) in each experiment. The reaction systems consisted of
 883 GUA (0.1 mM), DMB (0.01 mM), VL (0.01 mM), and AN (1 mM) under air-saturated conditions after 180 min of simulated
 884 sunlight irradiation. The UHPLC-HESI-Orbitrap-MS data were obtained in both positive (POS) and negative (NEG) ion
 885 modes.
 886

Exp no.	Reaction conditions	Initial GUA (and DMB or VL) decay rate constants ($\text{min}^{-1}/\text{s}^{-1}$) ^a	Normalized abundance of products ^b	Normalized abundance of N-containing compounds ^b	$\langle O:C \rangle^c$	$\langle H:C \rangle^c$	$\langle N:C \rangle^c$	$\langle OS_C \rangle^c$
1	GUA+DMB	GUA: 6.3 ± 0.25 DMB: 0.78 ± 0.10	376 \pm 22	NA	POS: 0.34	0.91	NA	-0.22
					NEG: 0.40	0.94	NA	-0.15
2	GUA+ DMB+AN	GUA: 5.3 ± 0.50 DMB: 0.69 ± 0.052	310 \pm 4	114	POS: 0.28	0.94	0.12	-0.03
					NEG: 0.37	0.91	0.04	-0.05
3	GUA+VL	GUA: 1.5 ± 0.14 VL: 3.6 ± 0.55	94 \pm 5	NA	POS: 0.41	0.91	NA	-0.10
					NEG: 0.40	0.94	NA	-0.14
4	GUA+ VL+AN	GUA: 1.6 ± 0.12 VL: 2.9 ± 0.032	100 \pm 2	8	POS: 0.31	1.02	0.02	-0.34
					NEG: 0.39	0.91	0.03	-0.02
5	GUA+AN	0.57 ± 0.036	23 \pm 1	9	POS: 0.35	0.99	0.16	0.19
					NEG: 0.38	1.01	0.05	-0.08

887

888 ^aThe data fitting was performed in the initial linear region. Each value is the average of results from triplicate experiments,
 889 corrected for internal light screening due to DMB, VL, and AN, and normalized to the experimental photon flux. Errors
 890 represent one standard deviation. ^bThe normalized product abundance was calculated using the data from UHPLC-HESI-
 891 Orbitrap-MS in the positive (POS) ion mode as the GUA signal from the negative (NEG) ion mode was weak, which may
 892 introduce significant uncertainties during normalization. The uncertainties were propagated from the changes in [GUA]
 893 measured using UHPLC-PDA and the MS signal intensities. The samples for experiments without AN (marked with NA)
 894 were not analyzed for N-containing compounds. ^cThe average elemental ratios ($\langle O:C \rangle$, $\langle H:C \rangle$, and $\langle N:C \rangle$) and $\langle OS_C \rangle$ were
 895 based on the UHPLC-HESI-Orbitrap-MS results and estimated using the signal-weighted method (Bateman et al., 2012).
 896 The OS_C of GUA, DMB, and VL are -0.57, -0.44, and -0.25, respectively.

897

898

899

900

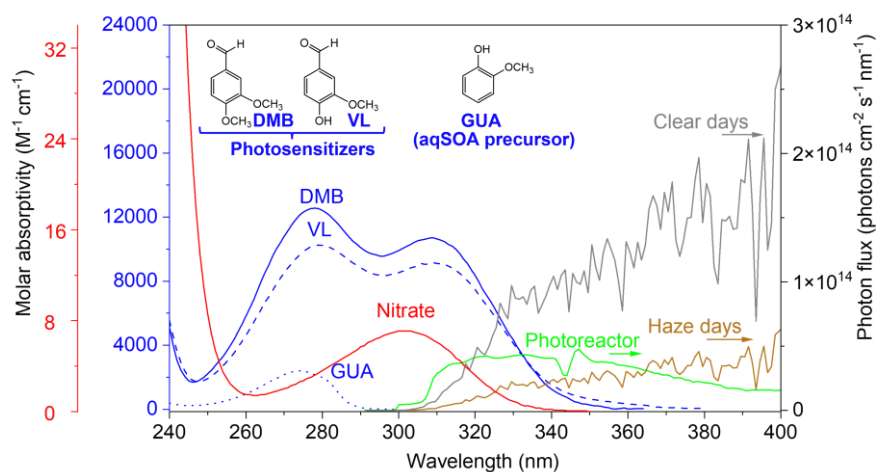
901

902

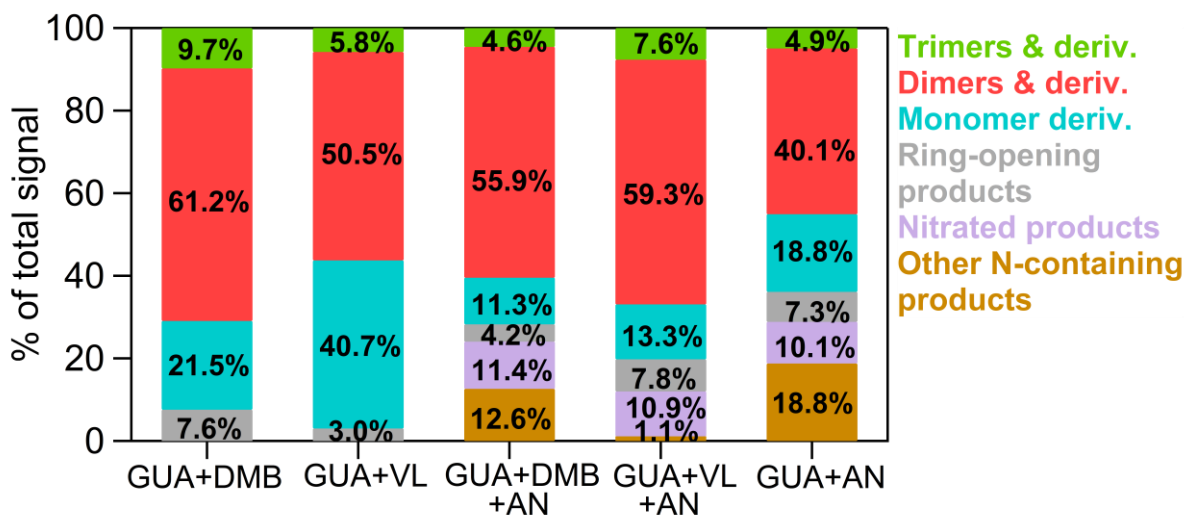
903

904

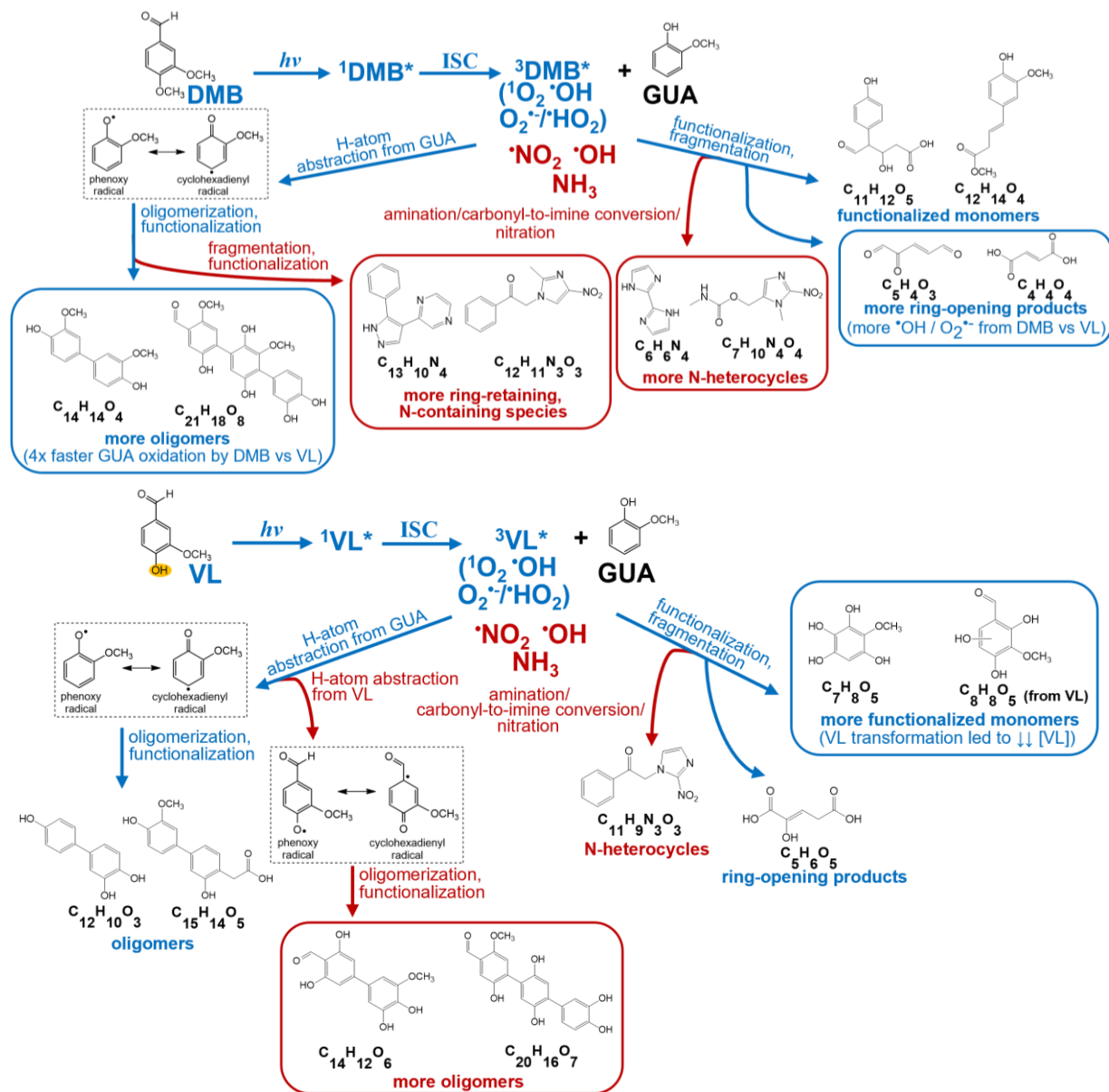
905
906
907
908
909
910
911
912
913
914



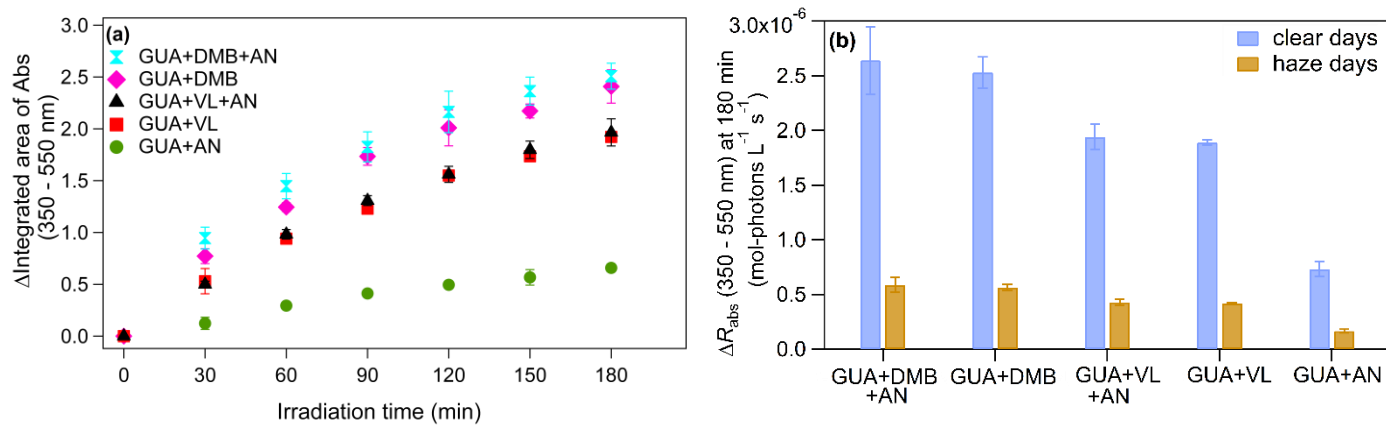
915 **Figure 1.** The base-10 molar absorptivities ($M^{-1} \text{ cm}^{-1}$) of 3,4-dimethoxybenzaldehyde (DMB, blue solid line), vanillin (VL, 916 blue dashed line), guaiacol (GUA, blue dotted line), and nitrate (red solid line). The green line is the photon flux in the 917 aqueous photoreactor. The gray and brown lines are the photon fluxes on typical clear and haze days, respectively, in 918 Beijing, China (Mabato et al., 2022). The top of the figure also shows the structures of DMB, VL, and GUA.



919 **Figure 2.** Signal-weighted distributions of aqSOA from GUA+DMB, GUA+VL, GUA+DMB+AN, GUA+VL+AN, and 920 GUA+AN. These product distributions were calculated from combined UHPLC-HESI-Orbitrap-MS data obtained in positive 921 (POS) and negative (NEG) ion modes. The values indicate the contribution of different product classifications to the total 922 signals for each reaction condition.



923 **Figure 3.** Summary of the main differences between photosensitized GUA oxidation by $^3\text{DMB}^*$ (top) and $^3\text{VL}^*$ (bottom) in
 924 the absence (blue labels and boxes) and presence (red labels and boxes) of ammonium nitrate at pH 4 under air-saturated
 925 conditions. Boxed structures indicate product classifications with notable differences. DMB and VL absorb light and are
 926 promoted to their singlet excited states ($^1\text{DMB}^*$ and $^1\text{VL}^*$), which then undergo intersystem crossing (ISC) to form $^3\text{DMB}^*$
 927 and $^3\text{VL}^*$. Secondary oxidants ($^1\text{O}_2$, $\text{O}_2^{\cdot-}/\text{HO}_2$, $\cdot\text{OH}$) can be formed from $^3\text{DMB}^*$ and $^3\text{VL}^*$ upon reactions with O_2 and GUA
 928 (George et al., 2018; Chen et al., 2020; Misovich et al., 2021; Mabato et al., 2022). The structures shown are examples of the
 929 major products (Tables S1 to S4) for different product classifications.



931

932

933

934 **Figure 4.** (a) Increase in light absorption throughout 180 min of irradiation for all reaction systems studied and (b) Change
 935 in the rate of sunlight absorption (ΔR_{abs}) from 350-550 nm at 180 min during typical clear and haze days in Beijing, China
 936 for aqSOA from GUA+DMB+AN, GUA+DMB, GUA+VL+AN, GUA+VL, and GUA+AN. Error bars represent one
 937 standard deviation of triplicate experiments.